



TITLE:

Entropy production in a longitudinally expanding Yang–Mills field with use of the Husimi function: semiclassical approximation

AUTHOR(S):

Matsuda, Hidefumi; Kunihiro, Teiji; Ohnishi, Akira; Takahashi, Toru T

CITATION:

Matsuda, Hidefumi ...[et al]. Entropy production in a longitudinally expanding Yang–Mills field with use of the Husimi function: semiclassical approximation. *Progress of Theoretical and Experimental Physics* 2022, 2022(7): 073D02.

ISSUE DATE:

2022-07

URL:

<http://hdl.handle.net/2433/278779>

RIGHT:

© The Author(s) 2022. Published by Oxford University Press on behalf of the Physical Society of Japan.; This is an Open Access article distributed under the terms of the Creative Commons Attribution License, which permits unrestricted reuse, distribution, and reproduction in any medium, provided the original work is properly cited.Funded by SCOAP3

Entropy production in a longitudinally expanding Yang–Mills field with use of the Husimi function: semiclassical approximation

Hidefumi Matsuda^{1,*}, Teiji Kunihiro², Akira Ohnishi², and Toru T. Takahashi³

¹*Department of Physics, Faculty of Science, Kyoto University, Kyoto 606-8502, Japan*

²*Yukawa Institute for Theoretical Physics, Kyoto University, Kyoto 606-8502, Japan*

³*National Institute of Technology, Gunma College, Gunma 371-8530, Japan*

*E-mail: da.matsu.00.bbb.kobe@gmail.com

Received March 14, 2022; Revised May 23, 2022; Accepted June 3, 2022

.....
We investigate the possible thermalization process of the highly occupied and weakly coupled Yang–Mills fields expanding along the beam axis through an evaluation of the entropy, particle number, and pressure anisotropy. The time evolution of the system is calculated by solving the equation of motion for the Wigner function in the semiclassical approximation with initial conditions mimicking the glasma. For the evaluation of the entropy, we adopt Husimi–Wehrl (HW) entropy, which is obtained by using the Husimi function, a positive semidefinite quantum distribution function given by smearing the Wigner function. By numerical calculations at $g = 0.1$ and 0.2 , the entropy production is found to occur together with the particle creation in two distinct stages: In the first stage, the particle number and entropy at low longitudinal momenta grow rapidly. In the second stage, the particle number and entropy of higher longitudinal momentum modes show a slower increase. The pressure anisotropy remains in our simulation and implies that the system is still out of equilibrium.
.....

Subject Index A51, B01, D28, D31

1. Introduction

Experimental studies at RHIC and LHC have provided phenomenological evidence of the formation of strongly coupled matter soon after the collisions of relativistic heavy ions, and its evolution is well described by the hydrodynamics. The shear viscosity of the fluid in these successful hydrodynamical models is so small [1–4] that the entropy produced in the hydrodynamical stage is estimated to be about only 10% of the total entropy [5,6]. Thus most of the entropy is expected to be created before the formation of the fluid [7]. We have, however, only a poor grasp of the physical mechanism of such early entropy production within the underlying quantum chromodynamics. Thus it is necessary to elucidate the entropy production mechanism in the pre-hydrodynamic stage for a deeper understanding of the outstanding problem of why the hydrodynamics becomes applicable a short time after the collisions, $\tau \sim 0.6\text{--}1$ fm/ c , known as the early thermalization puzzle [8].

Shortly after the contact between two nuclei, the matter produced is understood as a highly occupied system consisting of weakly coupled but strongly interacting gluons [9–13]. Such gluonic matter, called a glasma, initially consists of approximately boost-invariant color electric and color magnetic fields parallel to the collision axis. The fluctuations of these boost-invariant fields grow exponentially due to instabilities of the Yang–Mills theory [14–36]. The exponential

growth of fluctuations should play a role in the isotropization of pressure in the glasma [37,38], and is also expected to drive entropy production in the glasma [39,40]. Eventually, the grown Yang–Mills field is expected to decay into particles and to form a hydrodynamic fluid.

In order to investigate the real-time dynamics of the glasma, a semiclassical method is widely used [29,32,38,40–43]. In this method, the classical field equation of motion is solved starting from the initial conditions containing quantum fluctuations; this is implemented to evaluate the real-time evolution of a Wigner function, a Wigner–Weyl transform of a density matrix in terms of the field variables and their conjugate momenta. Such a semiclassical description can be applied to the real-time evolution of highly occupied and weakly coupled systems [43], where a quantum effect gives only a small contribution.

It should be noted that some kind of coarse-graining is necessary in order to discuss thermalization in terms of the entropy based on the density matrix, the Wigner function or the classical phase space distribution function defined microscopically. Exact quantum evolution of a density matrix $\hat{\rho}$ is unitary, and thereby the von Neumann entropy $S = -\text{Tr}\rho \ln \rho$ stays constant. Analogously, in classical systems, the phase space distribution function is constant along the classical trajectory and the Boltzmann entropy, $S = -\int dx dp / (2\pi)^D f \ln f$, with D and f being the number of degrees of freedom and the classical distribution function, stays constant due to Liouville’s theorem. One of the ways to perform coarse-graining is to use the entanglement entropy [44,45], the von Neumann entropy defined by a partially traced density matrix. The time evolution of the partially traced density matrix is non-unitary and then the entanglement entropy can grow in time. However, it is difficult to perform a partial trace for many-body systems such as field theory. Another way is to use the entropy defined by the smeared density matrix or the Wigner function. The Husimi function, a smeared Wigner function within the allowance of the uncertainty principle, is positive semidefinite and can be regarded as a probability density function in the phase space, and thus we can define the entropy based on the Husimi function, which we call the Husimi–Wehrl (HW) entropy [46–49]. The properties of the HW entropy both in and out of equilibrium have been studied analytically in some simple models: For a harmonic oscillator with a quantum $\hbar\omega$, the HW entropy for the Gibbs ensemble is larger than the von Neumann entropy but tends to agree with that in the classical/high-temperature limit ($\hbar/T \rightarrow 0$) [49]. In an inverted harmonic oscillator, the growth rate of the HW entropy asymptotically converges to the Kolmogorov–Sinai (KS) entropy, a sum of positive Lyapunov exponents [49], which implies that the production of the HW entropy is related to the chaoticity and instabilities in its classical counterpart. Both results suggest that the HW entropy can be a suitable guide to investigate thermalization at least in classical or semiclassical systems.

In this article, we evaluate the evolution of the Wigner function of the highly occupied and weakly coupled Yang–Mills fields with initial conditions mimicking the glasma in the semiclassical approximation, and analyze its thermalization in terms of the HW entropy that is obtained from the evaluated Wigner function. The semiclassical approximation method adopted here is essentially the same as the so-called classical statistical approximation [29,32,38,40–43] in the sense that the initial conditions are sampled by a Monte Carlo method and the classical equations of motion are solved. Our simulation is performed in the τ – η coordinate system, which represents a system expanding along the beam axis at the speed of light. In Refs. [39,40], the authors numerically showed that the HW entropy definitely grows by the classical dynamics of the Yang–Mills field, and that the growth rate of the HW entropy is related to the intrinsic dynamics of the Yang–Mills theory, such as the chaoticity and instabilities. It should be noted,

however, that the previous studies were only done in a static geometry with a focus on the thermalization by the intrinsic dynamics of the Yang–Mills field. Thus it would be intriguing to examine whether their findings are robust enough that they persist in an expanding geometry. The present work is an extension of the previous analysis to the expanding system with some technical improvements: We give an improved definition of the HW entropy in field theories that resolves two problems left unsolved in Refs. [39,40], over-counting gauge degrees of freedom and an ambiguity in the choice of smearing parameters. Another important development in this article is the evaluation of the particle number and its relevance to the entropy production. The initial condition, given as a glasma-like one with quantum fluctuations, may be described as a coherent state. Then the deviation from the coherent state is realized in the subsequent time evolution. We give an operator representation of the particle number created due to this deviation, and investigate the relation of the entropy and particle number production. Moreover we provide a theoretical basis of the numerical method for a precise evaluation of the HW entropy by the test particle method, which was proposed in Ref. [39].

This article is organized as follows. In Sect. 2, we introduce the semiclassical description of the real-time evolution of quantum systems based on the Wigner function, and give the definition of the HW entropy using a simple example: 1D quantum mechanics. In Sect. 3, we show how to numerically evaluate the HW entropy of a semiclassical field, using the scalar theory in the Minkowski spacetime. In Sect. 4, we investigate the dynamical production of the HW entropy in the semiclassical evolution of the $SU(2)$ Yang–Mills field in the expanding geometry. We also study other observables, pressure, and particle number, and discuss the relation between the HW entropy and them. In Sect. 5, we summarize this article.

2. Formalism

In this section, we introduce the semiclassical description of the real-time evolution of quantum systems based on the Wigner function, and give the definition of the HW entropy, using a 1D harmonic oscillator whose Hamiltonian reads $H = \hat{p}^2/2 + \omega^2 \hat{x}^2/2 = \omega(\hat{a}^\dagger \hat{a} + 1/2)$ with $\hat{a} = (\omega \hat{x} + i \hat{p})/\sqrt{2\omega}$.

2.1 Semiclassical description of the Wigner function

The Wigner function is defined as the Wigner–Weyl transform of the density matrix $\hat{\rho}(t)$,

$$f_W(x, p) \equiv \int dy \left\langle x + \frac{y}{2} \mid \hat{\rho}(t) \mid x - \frac{y}{2} \right\rangle e^{-ipy}. \quad (1)$$

To describe the semiclassical evolution of the Wigner function, we use the classical limit of the von Neumann equation,

$$\frac{\partial}{\partial t} f_W(x, p) = \lim_{\hbar \rightarrow 0} \{ \{ H, f_W(x, p) \} \}, \quad (2)$$

where $\{ \{, \} \}$ denotes the Moyal bracket. The Moyal bracket can be written as a power series of \hbar^2 ,

$$\{ \{ H, f_W(x, p) \} \} = \{ H, f_W(x, p) \} + \mathcal{O}(\hbar^2), \quad (3)$$

where $\{, \}$ denotes the Poisson bracket. In the classical limit ($\hbar \rightarrow 0$), therefore, Eq. (2) has the same form as the Liouville equation, which is an evolution equation of a classical distribution function:

$$\frac{\partial}{\partial t} f_W(x, p) = \{ H, f_W(x, p) \}. \quad (4)$$

By combining the classical evolution equation given by Eq. (4) with the semiclassical initial condition given later in Eq. (7), we can describe the time-dependent Wigner function within the semiclassical approximation, where quantum fluctuation effects up to $\mathcal{O}(\hbar^1)$ are included.

We calculate an expectation value of the given observable $\hat{O}(\hat{x}, \hat{p})$ through the following relation:

$$\langle \hat{O}(\hat{x}, \hat{p}) \rangle = \text{Tr} \left(\hat{O}(\hat{x}, \hat{p}) \hat{\rho} \right) = \int d\Gamma \mathcal{O}_W(x, p) f_W(x, p), \quad (5)$$

where $d\Gamma = dx dp / (2\pi)$ is the integration measure and $\mathcal{O}_W(x, p)$ is the Wigner–Weyl transform of $\hat{O}(\hat{x}, \hat{p})$,

$$\mathcal{O}_W(x, p) = \int dy \left\langle x + \frac{y}{2} \middle| \hat{O}(\hat{x}, \hat{p}) \middle| x - \frac{y}{2} \right\rangle e^{-ipy}. \quad (6)$$

In actual calculations in field theories, we may need to subtract the vacuum expectation value and others to obtain the well-defined observables as discussed later.

2.2 Wigner function of a coherent state

We use a coherent state for the initial condition in actual calculations discussed later, since a description with the use of a coherent state is useful when the semiclassical approximation is valid. A coherent state is an eigenstate of the annihilation operator $\hat{a}|\alpha\rangle = \alpha|\alpha\rangle$, and is represented as $|\alpha\rangle = e^{-|\alpha|^2/2} e^{\alpha \hat{a}^\dagger} |0\rangle$ with $|0\rangle$ being the perturbative vacuum state: $\hat{a}|0\rangle = 0$. The coherent state satisfies the minimum uncertainty relation, $\Delta x \Delta p = \frac{1}{2}$. With the use of the density matrix $\hat{\rho} := |\alpha\rangle\langle\alpha|$, the Wigner function of the coherent state $|\alpha\rangle$ is given by

$$f_W(x, p) = \int dy \left\langle x + \frac{y}{2} \middle| \alpha \right\rangle \left\langle \alpha \middle| x - \frac{y}{2} \right\rangle e^{-ipy} = 2 \exp \left[-\frac{(x - \bar{x})^2}{2(\Delta x)^2} - \frac{(p - \bar{p})^2}{2(\Delta p)^2} \right], \quad (7)$$

where \bar{x} and \bar{p} are the expectation values of the position and momentum, respectively, and are related to the eigenvalue as $\alpha = (\omega \bar{x} + i \bar{p}) / \sqrt{2\omega}$. The variances are given by $(\Delta x)^2 := \langle \alpha | (\hat{x} - \bar{x})^2 | \alpha \rangle = 1/(2\omega)$ and $(\Delta p)^2 := \langle \alpha | (\hat{p} - \bar{p})^2 | \alpha \rangle = \omega/2$.

2.3 Husimi–Wehrl entropy

The Husimi function is obtained by smearing the Wigner function in the phase space within the allowance of the uncertainty principle,

$$f_H(x, p, \sigma) \equiv \int d\Gamma' f_W(x', p') G(x - x', p - p', \sigma), \quad (8)$$

where $G(x, p, \sigma)$ is the Gaussian smearing function,

$$G(x, p, \sigma) = 2e^{-\sigma x^2 - p^2/\sigma}, \quad (9)$$

where σ is the smearing parameter. The Husimi function is normalized in the phase space as $\int d\Gamma f_H(x, p, \sigma) = 1$. In addition, it is given as the expectation value of the density matrix in a coherent state $|\alpha; \sigma\rangle$ defined as the eigenstate of the annihilation operator $\hat{a} = (\sigma \hat{x} + i \hat{p}) / \sqrt{2\sigma}$, $f_H(x, p, \sigma) = \langle \alpha; \sigma | \hat{\rho} | \alpha; \sigma \rangle$, and is positive semidefinite unlike the Wigner function. Therefore, the Husimi function can be regarded as a probability distribution function in the phase space. Then, we can define the Husimi–Wehrl entropy as

$$S_{\text{HW}}(\sigma) \equiv - \int d\Gamma f_H(x, p, \sigma) \ln f_H(x, p, \sigma). \quad (10)$$

While there exists an ambiguity of the choice of the smearing parameter σ in the Husimi function, we unambiguously fix σ by imposing a physically natural requirement in the later section.

3. Husimi–Wehrl entropy of a scalar field in a non-expanding geometry

Before proceeding with the study of the Yang–Mills field in the expanding geometry, we show how to numerically evaluate the HW entropy of a semiclassical field, using the scalar theory in Minkowski spacetime as an example. All quantities in this section are normalized by a spatial lattice spacing a .

3.1 Scalar field theory on a lattice

We consider the massless ϕ^4 theory on a L^3 lattice whose Hamiltonian is given by

$$H = \sum_x \left[\frac{1}{2} \hat{\pi}(x)^2 - \frac{1}{2} (\nabla^F \hat{\phi}(x))^2 + \frac{\lambda}{4!} \hat{\phi}^4(x) \right], \quad (11)$$

where $\nabla^F = (\partial_1^F, \partial_2^F, \partial_3^F)$ denotes a forward difference operator, and $\hat{\pi} = \hat{\phi}$ is the canonical conjugate variable of $\hat{\phi}$. Then, field variables for the free scalar field ($\lambda = 0$) on the lattice after the second quantization are given by

$$\hat{\phi}(x) = \frac{1}{\sqrt{L^3}} \sum_k \hat{\phi}_k e^{ik \cdot x} = \frac{1}{\sqrt{L^3}} \sum_k \frac{1}{\sqrt{2\omega_k}} \left(\hat{a}_k e^{-i\omega_k t} + \hat{a}_{-k}^\dagger e^{i\omega_k t} \right) e^{ik \cdot x}, \quad (12)$$

$$\hat{\pi}(x) = \frac{1}{\sqrt{L^3}} \sum_k \hat{\pi}_k e^{ik \cdot x} = \frac{-i}{\sqrt{L^3}} \sum_k \sqrt{\frac{\omega_k}{2}} \left(\hat{a}_k e^{-i\omega_k t} - \hat{a}_{-k}^\dagger e^{i\omega_k t} \right) e^{ik \cdot x}, \quad (13)$$

where $(\hat{\phi}_k, \hat{\pi}_k)$ are the Fourier transform of $(\hat{\phi}(x), \hat{\pi}(x))$, $\hat{a}_k (\hat{a}_k^\dagger)$ is the annihilation (creation) operator for the free scalar field satisfying $[\hat{a}_k, \hat{a}_{k'}^\dagger] = \delta_{k,k'}$, and $\omega_k = 2\sqrt{\sin^2(k_1/2) + \sin^2(k_2/2) + \sin^2(k_3/2)}$ is the eigenfrequency of the free field mode with momentum \mathbf{k} on the lattice.

The free part of the scalar theory can be interpreted as a set of harmonic oscillators, whose Hamiltonian is given by

$$H_{\text{free}} = \sum_k \omega_k \left(\hat{a}_k^\dagger \hat{a}_k + \frac{1}{2} \right) = \sum_k H_k^{\text{h.o.}}, \quad H_k^{\text{h.o.}} = \frac{1}{2} \hat{\Pi}_k^2 + \frac{1}{2} \omega_k^2 \hat{\Phi}_k^2, \quad (14)$$

where we have introduced new canonical variables for each momentum mode, $(\hat{\Phi}_k, \hat{\Pi}_k)$, utilizing the annihilation and creation operators as

$$\hat{\Phi}_k \equiv \frac{1}{\sqrt{2\omega_k}} \left[\hat{a}_k + \hat{a}_k^\dagger \right], \quad \hat{\Pi}_k \equiv -i \sqrt{\frac{\omega_k}{2}} \left[\hat{a}_k - \hat{a}_k^\dagger \right], \quad (15)$$

or, accordingly,

$$\hat{a}_k = (\omega_k \hat{\Phi}_k + i \hat{\Pi}_k) / \sqrt{2\omega_k}. \quad (16)$$

Now we can consider the Winger function $f_W(\{\Phi, \Pi\})$ expressed in terms of Φ_k and Π_k . As the initial condition, we adopt the coherent state $|\{\alpha_k\}\rangle$ that is the eigenstate of annihilation operators for the free scalar field, $\{\hat{a}_k\}$ and is given by the product of coherent states of each mode, $|\{\alpha_k\}\rangle = \prod_k |\alpha_k\rangle$. Accordingly, the density matrix is expressed as $\hat{\rho}(t) = |\{\alpha_k\}\rangle \langle \{\alpha_k\}| = \prod_k |\alpha_k\rangle \langle \alpha_k|$. Then, as shown in Eq. (7), the Winger function at the initial time is given by the Gaussian function,

$$\begin{aligned} f_W(\{\Phi, \Pi\}) &= \prod_k \int d\Phi'_k \left\langle \Phi_k + \frac{\Phi'_k}{2} \middle| \alpha_k \right\rangle \left\langle \alpha_k \middle| \Phi_k - \frac{\Phi'_k}{2} \right\rangle e^{-i\Pi_k \Phi'_k} \\ &= \prod_k 2 \exp \left[-\frac{(\Phi_k - \bar{\Phi}_k)^2}{2(\Delta\Phi_k)^2} - \frac{(\Pi_k - \bar{\Pi}_k)^2}{2(\Delta\Pi_k)^2} \right], \end{aligned} \quad (17)$$

where the expectation values $\bar{\Phi}_k$ and $\bar{\Pi}_k$ are the real and imaginary parts of the coherent state eigenvalue $\alpha_k = (\omega_k \bar{\Phi}_k + i\bar{\Pi}_k)/\sqrt{2\omega_k}$ and the variances $(\Delta\Phi_k)^2$ and $(\Delta\Pi_k)^2$ are determined by the eigenfrequency ω_k as $\omega_k = 1/[2(\Delta\Phi_k)^2] = 2(\Delta\Pi_k)^2$. It is noted that the spread of the initial Wigner function characterized by the widths $\Delta\Phi_k$ and $\Delta\Pi_k$ corresponds to the zero-point oscillation of the vacuum if fluctuations of fields are regarded as particles.

We further define a Husimi function f_H as a smeared Wigner function with the smearing parameters $\{\sigma_k\}$ set to eigenfrequencies $\{\omega_k\}$,

$$f_H(\{\Phi, \Pi, \omega\}) = \int \mathcal{D}\Gamma' f_W(\{\Phi', \Pi'\}) G(\{\Phi - \Phi', \Pi - \Pi', \omega\}), \quad (18)$$

where $\mathcal{D}\Gamma = \prod_k d\Phi_k d\Pi_k / (2\pi)$ is an integration measure and $G(\{\Phi, \Pi, \omega\})$ is the smearing function defined as the product of single Gaussian smearing functions given in Eq. (9),

$$G(\{\Phi, \Pi, \omega\}) = \prod_k G(\Phi_k, \Pi_k, \omega_k). \quad (19)$$

The HW entropy is finally given by

$$S_{HW}(\{\omega\}) = - \int \mathcal{D}\Gamma f_H(\{\Phi, \Pi, \omega\}) \ln f_H(\{\Phi, \Pi, \omega\}). \quad (20)$$

We here comment on the smearing parameter choice shown above. The HW entropy $S_{HW}(\{\omega\})$ defined with the smearing parameter $\{\omega\}$ exhibits two remarkable and physically natural features, as shown in Appendix D, at $\lambda = 0$: The HW entropy $S_{HW}(\{\omega\})$ agrees with the von Neumann entropy $S_{vN} = -\text{Tr}(\rho \ln \rho)$ in the high-temperature limit, and the HW entropy $S_{HW}(\{\omega\})$ per degrees of freedom in vacuum is unity, the minimum of the HW entropy. These two features may justify the adoption of the definition in weak-coupling calculations. In the later discussion of this section, we omit $\{\omega\}$ in the expression of the HW entropy of the scalar field: S_{HW} .

3.2 Numerical method

3.2.1 *Evaluation of the Wigner function using the test particle method.* In the actual evaluation of the Wigner function, we use the test particle (TP) method in which the Wigner function is approximated by a sum of the delta functions,

$$f_W^{\text{TP}}(\{\Phi, \Pi\}) = \frac{1}{N_{\text{TP}}} \sum_i \prod_k (2\pi) \delta(\Phi_k - \Phi_{k,i}(t)) \delta(\Pi_k - \Pi_{k,i}(t)), \quad (21)$$

where each delta function specifies the coordinate of an independent particle $(\Phi_{k,i}, \Pi_{k,i})$, which is generated so as to sample the classical field configurations (test particle configurations) according to the distribution of the Wigner function. The test particle method assumes the positive semidefiniteness of the Wigner function, which is certainly true in the time evolution of the Wigner function according to the Liouville equation shown in Eq. (4) starting from a positive definite initial condition like Eq. (17). The Wigner function given in Eq. (21) should give an accurate sampling of the original Wigner function in the large- N_{TP} limit.

The test particles at the initial time are generated according to the initial Wigner function given in Eq. (17),

$$\Phi_{k,i} = \bar{\Phi}_k + \sqrt{\frac{1}{2\omega_k}} \xi_{k,i}^R, \quad \Pi_{k,i} = \bar{\Pi}_k + \sqrt{\frac{\omega_k}{2}} \xi_{k,i}^I, \quad (22)$$

where $\xi_{k,i}^{R,I}$ are the random numbers obeying the normal Gaussian distribution. The time evolution of each test particle is obtained by the classical equation of motion, $\dot{\phi}(x) = \partial H / \partial \pi(x)$, $\dot{\pi}(x) = -\partial H / \partial \phi(x)$. Later, we calculate the expectation value of a given observable

$\hat{\mathcal{O}}(\{\hat{\Phi}, \hat{\Pi}\})$, such as pressure and particle number, by using the test particle expression of the Wigner function given in Eq. (5),

$$\langle \hat{\mathcal{O}}(\{\hat{\Phi}, \hat{\Pi}\}) \rangle = \frac{1}{N_{\text{TP}}} \sum_i \mathcal{O}(\{\Phi_i, \Pi_i\}). \quad (23)$$

3.2.2 Husimi–Wehrl entropy in the test particle method. By substituting the Wigner function given in Eq. (21) into Eq. (18), we obtain the Husimi function in the test particle method,

$$f_{\text{H}}^{\text{TP}}(\{\Phi, \Pi\}) = \frac{1}{N_{\text{TP}}} \sum_i \prod_k G_{k,i}(\Phi_k, \Pi_k), \quad (24)$$

$$G_{k,i}(\Phi_k, \Pi_k) = G(\Phi_k - \Phi_{k,i}(t), \Pi_k - \Pi_{k,i}(t), \omega_k). \quad (25)$$

Then the HW entropy in the test particle method is given by

$$S_{\text{HW}}^{\text{TP}} = - \int D\Gamma \left[\frac{1}{N_{\text{TP}}} \sum_i \prod_k G_{k,i}(\Phi_k, \Pi_k) \right] \ln \left[\frac{1}{N_{\text{TP}}} \sum_j \prod_{k'} G_{k',j}(\Phi_{k'}, \Pi_{k'}) \right]. \quad (26)$$

The HW entropy is evaluated in the following three steps in our test particle method, which is elaborated from that adopted in the previous works [39,40]. In the first step, we apply identical test particle sets to functions both inside and outside the logarithmic function in Eq. (26), and evaluate the HW entropy. We call this prescription the “single test particle method (sTP)”, and denote the HW entropy obtained by the sTP method as $S_{\text{HW}}^{\text{sTP}}$. In the second step, we compute the HW entropy using two different test particle sets for functions inside and outside the logarithmic function in Eq. (26). We call the second prescription the “parallel test particle method (pTP)”, and denote the HW entropy obtained by the pTP method as $S_{\text{HW}}^{\text{pTP}}$. Finally, we estimate the HW entropy by averaging $S_{\text{HW}}^{\text{sTP}}$ and $S_{\text{HW}}^{\text{pTP}}$, $S_{\text{HW}}^{\text{aTP}} \equiv (S_{\text{HW}}^{\text{sTP}} + S_{\text{HW}}^{\text{pTP}})/2$. As proven in Appendix C, we obtain the following inequality:

$$S_{\text{HW}}^{\text{sTP}} < S_{\text{HW}} < S_{\text{HW}}^{\text{pTP}} \quad (27)$$

by assuming that the numerical errors of the Husimi function, $\Delta^{\text{TP}} = f_{\text{H}}^{\text{TP}} - f_{\text{H}} \propto 1/\sqrt{N_{\text{TP}}}$, are sufficiently small due to the large value of N_{TP} , and that the odd-order contributions of Δ^{TP} to $S_{\text{HW}}^{\text{sTP}}$ and $S_{\text{HW}}^{\text{pTP}}$ disappear due to the numerical error cancellation. Moreover, it is also shown in Appendix C that the numerical errors proportional to N_{TP}^{-1} cancel each other out in $S_{\text{HW}}^{\text{aTP}}$, and $S_{\text{HW}}^{\text{aTP}}$ only contains $\mathcal{O}(N_{\text{TP}}^{-2})$ errors. Thus, for sufficiently large N_{TP} , the following nice equality holds:

$$S_{\text{HW}}^{\text{aTP}} = S_{\text{HW}} + \mathcal{O}(N_{\text{TP}}^{-2}). \quad (28)$$

In the next section, we numerically calculate $S_{\text{HW}}^{\text{sTP}}$, $S_{\text{HW}}^{\text{pTP}}$, and $S_{\text{HW}}^{\text{aTP}}$ at different numbers of test particles, and discuss the validity of Eqs. (27) and (28).

3.2.3 Product ansatz. We need to make a further approximation, assuming the product ansatz for the Wigner function in order to obtain the HW entropy in Eq. (26) in the test particle method. While the Husimi function is equivalent to the expectation value of the density matrix in the coherent state and takes a value $0 \leq f_{\text{H}} \leq 1$, the Husimi function in the test particle method, Eq. (24), takes a value $f_{\text{H}} \geq 2^{N_D}/N_{\text{TP}}$ at one of the test particle phase space coordinates, $(\Phi_k, \Pi_k) = (\Phi_{k,i}, \Pi_{k,i})$, with $N_D = L^3$ being the number of degrees of freedom. Then the required number of test particles is $N_{\text{TP}} > 2^{N_D}$ in order to respect the f_{H} range. As in this

example, in order to cover the $2N_D$ -dimensional phase space, we need a huge number of test particles. We cannot prepare such sufficiently large numbers of test particle configurations for large L .

To circumvent this practical problem, we assume the product ansatz for the Wigner function, *à la* the Hartree–Fock approach,

$$f_W(\{\Phi, \Pi\}) = \prod_k f_W^k(\Phi_k, \Pi_k), \quad f_W^k(\Phi_k, \Pi_k) = \frac{1}{N_{\text{TP}}} \sum_i (2\pi) \delta(\Phi_k - \Phi_{k,i}) \delta(\Pi_k - \Pi_{k,i}), \quad (29)$$

which means that there is no correlation between the wave functions of different momentum modes. Under the product ansatz, the Husimi function is also nicely expressed as the product of that of the single momentum mode,

$$f_H(\{\Phi, \Pi\}) = \prod_k f_H^k(\Phi_k, \Pi_k), \quad f_H^k(\Phi_k, \Pi_k) = \frac{1}{N_{\text{TP}}} \sum_i G_{k,i}(\Phi_k, \Pi_k), \quad (30)$$

which allows us to treat the multiple integration in Eq. (26) as the sum of double integrations,

$$S_{\text{HW}} = \sum_k S_{\text{HW}}^k, \quad S_{\text{HW}}^k = - \int \frac{d\Phi_k d\Pi_k}{(2\pi)^3} f_H^k(\Phi_k, \Pi_k) \ln f_H^k(\Phi_k, \Pi_k). \quad (31)$$

The product ansatz does not necessarily hold in interacting systems, since the interaction generates correlations between different modes. The product ansatz for f_H in Eq. (30) tells us that f_H^k is a partially traced distribution function,

$$f_H^k(\Phi_k, \Pi_k) = \int \prod_{k' \neq k} \frac{d\Phi_{k'} d\Pi_{k'}}{2\pi} f_H(\{\Phi, \Pi\}). \quad (32)$$

Thus, while we aim at calculating the entropy from the coarse-graining, the HW entropy with the product ansatz given in Eq. (31) is found to overestimate it by the amount of the entropy resulting from the loss of the correlation caused by the partial trace of f_H . So far, the entropy increase caused by the use of the product ansatz has been tested only for a few-dimensional quantum system [39], and the entropy increase in such a case is found to be around 20% of that from only the coarse-graining. However, the product ansatz is a kind of a mean-field approximation like the Hartree(–Fock) approximation and is expected to provide a good approximation for a system with large degrees of freedom, such as a highly occupied system, where fluctuations should be small.

3.3 Numerical results

Here we show the numerical results of the time evolution of the HW entropy of the scalar field theory using the product ansatz with a coupling constant $\lambda = 1$ on a 16^3 lattice with a periodic boundary condition. The initial positions of test particles in the phase space are generated according to the initial Wigner function given in Eq. (17), where the initial macroscopic fields $(\bar{\Phi}_k, \bar{\Pi}_k)$ are given so as to satisfy the following simple initial condition:

$$\bar{\Phi}(\mathbf{x}) = 5 \sin\left(\frac{\pi}{4}(x+y)\right), \quad \bar{\Pi}(\mathbf{x}) = 0. \quad (33)$$

The classical equation of motion for each test particle is solved by leapfrog integration. The number of test particles is taken as $N_{\text{TP}} = 160, 240, \text{ and } 320$.

Figure 1 shows the evolution of $S_{\text{HW}}^{\text{sTP}}$, $S_{\text{HW}}^{\text{pTP}}$, and $S_{\text{HW}}^{\text{aTP}}$ per degrees of freedom at $N_{\text{TP}} = 160, 240, \text{ and } 320$. It is found that $S_{\text{HW}}^{\text{sTP}} < S_{\text{HW}}^{\text{pTP}}$ always holds and the difference between $S_{\text{HW}}^{\text{sTP}}$ and $S_{\text{HW}}^{\text{pTP}}$ becomes smaller as N_{TP} increases, which is consistent with the inequality shown in Eq. (27). Moreover, the N_{TP} dependence of $S_{\text{HW}}^{\text{aTP}}$ at $N_{\text{TP}} = 160, 240, \text{ and } 320$ is much smaller

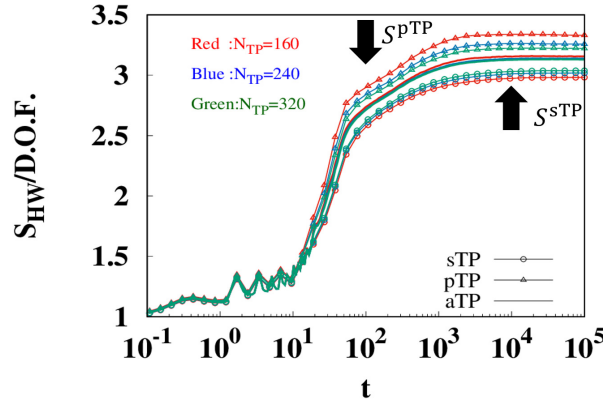


Fig. 1. The time evolution of the HW entropy of a scalar field with $\lambda = 1$ on a 16^3 lattice. The red, blue, and green lines show the results for $N_{\text{TP}} = 160, 240,$ and $320,$ respectively. The lines with circles, triangles, and no symbols show the HW entropy evaluated by the sTP method ($S_{\text{HW}}^{\text{sTP}}$), the pTP method ($S_{\text{HW}}^{\text{pTP}}$), and their average ($S_{\text{HW}}^{\text{aTP}}$), respectively.

than those for $S_{\text{HW}}^{\text{sTP}}$ and $S_{\text{HW}}^{\text{pTP}}$, and is only less than 2%, which indicates that the equality shown in Eq. (28) holds. In what follows, we adopt $S_{\text{HW}}^{\text{aTP}}$ as the estimation of S_{HW} , $S_{\text{HW}} = S_{\text{HW}}^{\text{aTP}}$.

The time evolution of the HW entropy shows the relaxation processes from a coherent state to thermal equilibrium. At the initial time $t = 0$, S_{HW} starts from unity, which reflects that the initial system is given by a coherent state. One sees that S_{HW} first increases rapidly, then shows only a gradual increase, and finally reaches some value and hardly changes. The saturation of S_{HW} indicates that the system reaches thermal equilibrium. The final value of S_{HW} may be the HW entropy in the thermal equilibrium in the classical limit, which is estimated as

$$S_{\text{HW}}^{\text{cl.eq.}} \sim 3.1. \quad (34)$$

To compare with the thermal HW entropy shown in Eq. (34), we consider the classical Gibbs ensemble of the free field,

$$f_{\text{W}}^{\text{cl.eq.}}(\{\Phi, \Pi\})|_{\lambda=0} \propto e^{-H_{\text{free}}/T} = \prod_k \exp\left[-\frac{\omega_k^2 \Phi_k^2 + \Pi_k^2}{2T}\right], \quad (35)$$

which gives thermal expectation values of observables in the classical limit at $\lambda = 0$. Then, we get the Husimi function,

$$f_{\text{H}}^{\text{cl.eq.}}(\{\Phi, \Pi, \omega\})|_{\lambda=0} \propto \prod_k \exp\left[-\frac{\omega_k^2 \Phi_k^2 + \Pi_k^2}{2(T + \omega_k/2)}\right], \quad (36)$$

and the HW entropy,

$$S_{\text{HW}}^{\text{cl.eq.}}|_{\lambda=0} = \sum_k \left[1 + \ln\left(\frac{T + \omega_k/2}{\omega_k}\right)\right]. \quad (37)$$

Assuming that the system is in thermal equilibrium after the HW entropy stops increasing, we extract the temperature of the system through the equipartition relation $\langle \pi(x)^2 \rangle = T$ that holds in thermal equilibrium in the classical limit. By substituting the numerically extracted temperature $T = 20$ into Eq. (37), we obtain $S_{\text{HW}}^{\text{cl.eq.}}|_{\lambda=0}$ at the same temperature as our simulation, $S_{\text{HW}}^{\text{cl.eq.}}|_{\lambda=0, T=20} \sim 3.2$. This theoretical estimate and our numerical estimation $S_{\text{HW}}^{\text{cl.eq.}}|_{\lambda=1, T=20} \sim 3.1$ in Eq. (34) agree well with each other, and this indicates that our simulation parameter at $\lambda = 1$ describes the relaxation to thermal equilibrium in the weak-coupling

region of the theory. Note that since the HW entropy shown in Eq. (37) is based on the classical thermal equilibrium distribution, its entropy density has UV divergence in the continuum limit. To circumvent this problem, it is useful to use a framework that can perturbatively take account of higher-order quantum effects, including quantum statistical properties, such as the kinetic theory [50] and the two-particle irreducible (2PI) effective action approach [51–53]. Aside from these descriptions, several improved classical field methods have been proposed to manage the UV divergence: introducing counterterms [54–56], integrating high-momentum modes assumed to be a heat bath [57,58], taking account of the explicit coupling of fields and particles [59,60], and considering a classical field theory with a quantum statistical nature [61].

4. Husimi–Wehrl entropy of the Yang–Mills field in an expanding geometry

Here we investigate the dynamical production of the HW entropy in the semiclassical time evolution of the SU(2) Yang–Mills field in the expanding geometry. We also compute the pressure and particle number, and discuss the relation between the HW entropy and them. We make all the quantities dimensionless normalizing with the transverse spatial lattice spacing a , and the η -direction gauge field A_η is normalized by the spatial lattice spacing a_η in the η -direction.

4.1 Formulation

The evolution of the longitudinally expanding system is discussed using the τ – η coordinate $(x^\tau, x^1, x^2, x^\eta) = (\tau = \sqrt{t^2 - z^2}, x, y, \eta = \frac{1}{2} \ln \frac{t+z}{t-z})$ with the metric $g_{\mu\nu} = \text{diag}(1, -1, -1, -\tau^2)$. We consider a non-compact Hamiltonian in the Fock–Schwinger gauge $A_\tau = 0$ on an $L_\perp^2 \times L_\eta$ lattice,

$$H = \frac{1}{2a_\eta\tau} \sum_{a,x} [(\hat{E}^{a1}(x)^2 + \hat{E}^{a2}(x)^2 + \hat{B}^{a1}(x)^2 + \hat{B}^{a2}(x)^2) + (a_\eta\tau)^2 (\hat{E}^{a\eta}(x)^2 + \hat{B}^{a\eta}(x)^2)]. \quad (38)$$

The color electric and color magnetic fields are defined as

$$\begin{aligned} \hat{E}^{ai}(x) &= a_\eta\tau \partial_\tau \hat{A}_i^a(x) \quad (i = 1, 2), \quad \hat{E}^{a\eta}(x) = \frac{1}{a_\eta\tau} \partial_\tau \hat{A}_\eta^a(x), \quad (39) \\ \hat{B}^{ai}(x) &= \frac{1}{2} \epsilon^{ijk} \left[\partial_j^F \hat{A}_k^a(x) - \partial_k^F \hat{A}_j^a(x) - \frac{g^2}{4} f^{abc} (\hat{A}_j^b(x) + \hat{A}_j^b(x + \hat{k})) (\hat{A}_k^c(x) + \hat{A}_k^c(x + \hat{j})) \right] \\ &\quad \times (i = 1, 2, \eta), \quad (40) \end{aligned}$$

where \hat{i} is the unit vector in the i -direction on the lattice. Here we show the expression of the gauge field in terms of the annihilation and creation operators for the free Yang–Mills field [42,62], which is shown in Appendix A,

$$\hat{A}_\mu^a(x) = \frac{1}{\sqrt{L_\perp^2 L_\eta}} \sum_{\lambda,k} \left(\hat{a}_k^{a\lambda} \tilde{A}_{\mu,k}^\lambda(\tau) e^{i(k_\perp \cdot x_\perp + \nu\eta)} + \text{h.c.} \right), \quad (41)$$

$$\tilde{A}_{\mu,k}^1(\tau) = \frac{i}{\omega_{k_\perp}} \sqrt{\frac{\pi}{4a_\eta}} e^{\frac{\pi|\tilde{\nu}|}{2a_\eta}} (0, \tilde{k}_2, \tilde{k}_1, 0) H_{i|\tilde{\nu}|/a_\eta}^{(2)}(\omega_{k_\perp} \tau), \quad (42)$$

$$\tilde{A}_{\mu,k}^2(\tau) = -\frac{\tilde{\nu}^*}{a_\eta \omega_{k_\perp}} \sqrt{\frac{\pi}{4a_\eta}} e^{\frac{\pi|\tilde{\nu}|}{2a_\eta}} \left(0, \tilde{k}_1 \alpha_{i|\tilde{\nu}|/a_\eta}^{(2)}(\omega_{k_\perp} \tau), \tilde{k}_2 \alpha_{i|\tilde{\nu}|/a_\eta}^{(2)}(\omega_{k_\perp} \tau), -\frac{a_\eta^2}{\tilde{\nu}^*} \beta_{i|\tilde{\nu}|/a_\eta}^{(2)}(\omega_{k_\perp} \tau) \right), \quad (43)$$

$$\alpha_{i|\tilde{\nu}|/a_\eta}^{(2)}(\omega_{k_\perp} \tau) = \int_{\omega_{k_\perp} \tau_0}^{\omega_{k_\perp} \tau} dz \frac{1}{z} H_{i|\tilde{\nu}|/a_\eta}^{(2)}(z) - \frac{\omega_{k_\perp} \tau_0}{(|\tilde{\nu}|/a_\eta)^2 + (\omega_{k_\perp} \tau_0)^2} \dot{H}_{i|\tilde{\nu}|/a_\eta}^{(2)}(\omega_{k_\perp} \tau_0), \quad (44)$$

$$\beta_{i|\tilde{\nu}|/a_\eta}^{(2)}(\omega_{k_\perp}\tau) = \int_{\omega_{k_\perp}\tau_0}^{\omega_{k_\perp}\tau} dz z H_{i|\tilde{\nu}|/a_\eta}^{(2)}(z) - \frac{(\omega_{k_\perp}\tau_0)^3}{(|\tilde{\nu}|/a_\eta)^2 + (\omega_{k_\perp}\tau_0)^2} \dot{H}_{i|\tilde{\nu}|/a_\eta}^{(2)}(\omega_{k_\perp}\tau_0), \quad (45)$$

where $\omega_{k_\perp} = 2\sqrt{\sin^2(\frac{k_1}{2}) + \sin^2(\frac{k_2}{2})}$ is a transverse frequency on the lattice; $\tilde{k}_i = 2e^{i\frac{k_i}{2}} \sin \frac{k_i}{2}$ ($i = 1, 2$) and $\tilde{\nu} = 2e^{i\frac{\nu}{2}} \sin \frac{\nu}{2}$ are the discrete Fourier transforms of the forward difference operators in the i -direction and η -direction, ∂_i^F and ∂_η^F , on the lattice; $H^{(2)}$ is the Hankel function of the second kind; and τ_0 is the initial proper time in our simulations. Here the residual gauge degrees of freedom are fixed by the Coulomb type gauge condition, $(\partial_1 A_1 + \partial_2 A_2 + \tau^{-2} \partial_\eta A_\eta) \Big|_{\tau=\tau_0} = 0$ [42]. Then the electric field, \hat{E} , and the free part of the magnetic field, \hat{B}_0 , can also be expressed in terms of \hat{a}_k^{λ} ,

$$\hat{E}^{ai}(x) = \frac{1}{\sqrt{L_\perp^2 L_\eta}} \sum_{\lambda, k} \left(\hat{a}_k^{\lambda} \mathcal{E}_k^{\lambda, i}(\tau) e^{i(k_\perp \cdot x_\perp + \nu \eta)} + \text{h.c.} \right), \quad (46)$$

$$\hat{B}_0^{ai}(x) = \epsilon^{ijk} \partial_j^F A_k(x) = \frac{1}{\sqrt{L_\perp^2 L_\eta}} \sum_{\lambda, k} \left(\hat{a}_k^{\lambda} \mathcal{B}_k^{\lambda, i}(\tau) e^{i(k_\perp \cdot x_\perp + \nu \eta)} + \text{h.c.} \right), \quad (47)$$

$$\mathcal{E}_k^{1, i}(\tau) = \dot{H}_{i|\tilde{\nu}|/a_\eta}^{(2)}(\omega_{k_\perp}\tau) \epsilon_k^{1, i}, \quad \mathcal{E}_k^{2, i}(\tau) = H_{i|\tilde{\nu}|/a_\eta}^{(2)}(\omega_{k_\perp}\tau) \epsilon_k^{2, i}, \quad (48)$$

$$\mathcal{B}_k^{1, i}(\tau) = H_{i|\tilde{\nu}|/a_\eta}^{(2)}(\omega_{k_\perp}\tau) \epsilon_k^{2, i*}, \quad \mathcal{B}_k^{2, i}(\tau) = \dot{H}_{i|\tilde{\nu}|/a_\eta}^{(2)}(\omega_{k_\perp}\tau) \epsilon_k^{1, i*}, \quad (49)$$

$$\epsilon_k^{1, i} = ia_\eta \tau \sqrt{\frac{\pi}{4a_\eta}} e^{\frac{\pi|\tilde{\nu}|}{2a_\eta}} (\tilde{k}_2^*, -\tilde{k}_1^*, 0), \quad \epsilon_k^{2, i} = -\frac{\tilde{\nu}^*}{\omega_{k_\perp}} \sqrt{\frac{\pi}{4a_\eta}} e^{\frac{\pi|\tilde{\nu}|}{2a_\eta}} \left(\tilde{k}_1, \tilde{k}_2, -\frac{\omega_{k_\perp}^2}{\tilde{\nu}^*} \right). \quad (50)$$

By substituting Eqs. (46) and (47) for the electric field and magnetic field in Eq. (38) respectively, we can obtain the free part of the Hamiltonian as

$$H_{\text{free}} = \sum_{a, \lambda, k} |\Delta_k| \left(\hat{a}_k^{\lambda\dagger} \hat{a}_k^{\lambda} + \frac{1}{2} \right) + \frac{1}{2} \sum_{a, \lambda, k} \left(\Delta_k \hat{a}_k^{\lambda} \hat{a}_{-k}^{\lambda} + \Delta_k^* \hat{a}_k^{\lambda\dagger} \hat{a}_{-k}^{\lambda\dagger} \right), \quad (51)$$

$$\Delta_k = \frac{\pi\tau}{4} e^{\frac{\pi|\tilde{\nu}|}{a_\eta}} \left((\omega_{k_\perp}^2 + |\tilde{\nu}/(\tau a_\eta)|^2) \left\{ H_{i|\tilde{\nu}|/a_\eta}^{(2)}(\omega_{k_\perp}\tau) \right\}^2 + (\omega_{k_\perp})^2 \left\{ \dot{H}_{i|\tilde{\nu}|/a_\eta}^{(2)}(\omega_{k_\perp}\tau) \right\}^2 \right). \quad (52)$$

The first term of Eq. (51) is asymptotically regarded as a set of harmonic oscillators,

$$\sum_{a, \lambda, k} |\Delta_k| \hat{a}_k^{\lambda\dagger} \hat{a}_k^{\lambda} \longrightarrow \sum_{a, \lambda, k} \omega_{k_\perp} \hat{a}_k^{\lambda\dagger} \hat{a}_k^{\lambda}, \quad (53)$$

and thus we can define canonical variables that are asymptotically regarded as harmonic oscillators,

$$\hat{\Phi}_k^{a\lambda} \equiv \frac{1}{\sqrt{2\omega_{k_\perp}}} \left[\hat{a}_k^{a\lambda} + \hat{a}_k^{a\lambda\dagger} \right], \quad (54)$$

$$\hat{\Pi}_k^{a\lambda} \equiv -i\sqrt{\frac{\omega_{k_\perp}}{2}} \left[\hat{a}_k^{a\lambda} - \hat{a}_k^{a\lambda\dagger} \right]. \quad (55)$$

In the same way as the scalar field, we consider the Wigner function for newly defined canonical variables $\{\hat{\Phi}, \hat{\Pi}\}$, whose initial condition is given by the product of coherent states of each mode, $|\{\alpha_k^{a, \lambda}\}\rangle = \prod_{a, \lambda, k} |\alpha_k^{a, \lambda}\rangle$,

$$f_W(\{\Phi, \Pi\}) = \prod_{a, \lambda, k} \int d\Phi_k^{a\lambda} \left\langle \Phi_k^{a\lambda} + \frac{\Phi_k^{a\lambda}}{2} \middle| \alpha_k^{a\lambda} \right\rangle \left\langle \alpha_k^{a\lambda} \middle| \Phi_k^{a\lambda} - \frac{\Phi_k^{a\lambda}}{2} \right\rangle e^{-i\Pi_k^{a\lambda} \Phi_k^{a\lambda}}. \quad (56)$$

We also consider the Husimi function and HW entropy for $\{\hat{\Phi}, \hat{\Pi}\}$ with smearing parameters that are taken as the same values as the asymptotic eigenfrequencies $\{\omega_{k_\perp}\}$, $f_H(\{\Phi, \Pi, \omega_\perp\})$ and

$S_{\text{HW}}(\{\omega_{\perp}\})$. Later, we omit $\{\omega_{\perp}\}$ in the expression of the HW entropy of the Yang–Mills field: S_{HW} .

4.2 Numerical results

Here we investigate the semiclassical evolution of the pressure, the HW entropy, and the distribution function of particles in the Yang–Mills theory on a $32^2 \times 420$ lattice with a periodic boundary condition. The coupling constant is taken as $g = 0.1$ and 0.2 and the longitudinal size of the system is taken as $V_{\eta} (= L_{\eta} \times a_{\eta}) = 2$. The test particle positions in the phase space at $\tau = \tau_0$ are generated randomly according to the initial Wigner function shown in Eq. (56). It is shown in the next paragraph how to give the initial macroscopic fields $(\bar{\Phi}_k^{a\lambda}, \bar{\Pi}_k^{a\lambda})$. The classical equation of motion for each test particle is solved by leapfrog integration. The number of test particles is taken as $N_{\text{TP}} = 96$.

We prepare the initial macroscopic fields so as to mimic the glasma initial condition [9–13] as follows: the color electric and color magnetic fields are boost invariant and parallel to the collision axis as

$$|\langle \hat{a}_k^{a\lambda} \rangle|_{\tau=\tau_0}^2 = \delta_{a,1} \left(\frac{V_{\eta}}{2\pi} \delta_{v,0} \right) \frac{\Delta}{\alpha_s} \cdot |f(\omega_{k_{\perp}})|^2, \quad (57)$$

$$\langle \hat{a}_k^{a\lambda} \rangle_{\tau=\tau_0} = \langle \hat{a}_{-k}^{a\lambda\dagger} \rangle_{\tau=\tau_0}, \quad (58)$$

where Δ is an arbitrary free parameter and $f(\omega_{k_{\perp}})$ is the transverse momentum distribution. The boost invariance is guaranteed by $\frac{V_{\eta}}{2\pi} \delta_{v,0}$, which is the lattice representation of the delta function $\delta(v)$. The phase of $\langle \hat{a}_k^{a\lambda} \rangle$ varies randomly. Since the direction of $\langle \hat{a}_k^{a\lambda} \rangle$ in the color space is toward the 1-direction, the gauge field is also directed toward the 1-direction in the color space, $\langle \hat{A}_k^{\lambda} \rangle \propto \delta_{a,1}$. Thus, the initial macroscopic magnetic field turns out to be equal to its free part shown in Eq. (47), $\langle \hat{B} \rangle_{\tau=\tau_0} = \langle \hat{B}_0 \rangle_{\tau=\tau_0}$. Here, we assume that all the contributions of fluctuations in $\langle \hat{B} \rangle_{\tau=\tau_0}$ are subtracted as the vacuum contribution or other divergences. Then, by substituting Eq. (57) into Eqs. (47) and (46) and utilizing Eq. (58), we obtain the analytic expression of nonzero parts of $\langle \hat{B}_k \rangle$ and $\langle \hat{E}_k \rangle$ as

$$\langle \hat{E}_k^{a1} \rangle_{a=1, v=0} = \langle \hat{a}_k^{1\lambda} \rangle_{\tau=\tau_0} \cdot (ia_{\eta} \tau_0 \tilde{k}_2^*) \sqrt{\frac{\pi}{4a_{\eta}}} \text{Re} \left(\dot{H}_0^{(2)}(\omega_{k_{\perp}} \tau_0) \right), \quad (59)$$

$$\langle \hat{E}_k^{a2} \rangle_{a=1, v=0} = \langle \hat{a}_k^{1\lambda} \rangle_{\tau=\tau_0} \cdot (ia_{\eta} \tau_0 \tilde{k}_1^*) \sqrt{\frac{\pi}{4a_{\eta}}} \text{Re} \left(\dot{H}_0^{(2)}(\omega_{k_{\perp}} \tau_0) \right), \quad (60)$$

$$\langle \hat{E}_k^{a\eta} \rangle_{a=1, v=0} = \langle \hat{a}_k^{2\lambda} \rangle_{\tau=\tau_0} \cdot \omega_{k_{\perp}} \sqrt{\frac{\pi}{4a_{\eta}}} \text{Re} \left(H_0^{(2)}(\omega_{k_{\perp}} \tau_0) \right), \quad (61)$$

$$\langle \hat{B}_k^{a1} \rangle_{a=1, v=0} = \langle \hat{a}_k^{2\lambda} \rangle_{\tau=\tau_0} \cdot (ia_{\eta} \tau_0 \tilde{k}_2^*)^* \sqrt{\frac{\pi}{4a_{\eta}}} \text{Re} \left(\dot{H}_0^{(2)}(\omega_{k_{\perp}} \tau_0) \right), \quad (62)$$

$$\langle \hat{B}_k^{a2} \rangle_{a=1, v=0} = \langle \hat{a}_k^{2\lambda} \rangle_{\tau=\tau_0} \cdot (ia_{\eta} \tau_0 \tilde{k}_1^*)^* \sqrt{\frac{\pi}{4a_{\eta}}} \text{Re} \left(\dot{H}_0^{(2)}(\omega_{k_{\perp}} \tau_0) \right), \quad (63)$$

$$\langle \hat{B}_k^{a\eta} \rangle_{a=1, v=0} = \langle \hat{a}_k^{1\lambda} \rangle_{\tau=\tau_0} \cdot \omega_{k_{\perp}} \sqrt{\frac{\pi}{4a_{\eta}}} \text{Re} \left(H_0^{(2)}(\omega_{k_{\perp}} \tau_0) \right). \quad (64)$$

On account of the formula

$$\text{Re} H_0^{(2)}(z) = 1 - \frac{z^2}{4} + \mathcal{O}(z^3),$$

the transverse components of $\langle \hat{\mathbf{B}}_k \rangle$ and $\langle \hat{\mathbf{E}}_k \rangle$ are proportional to $(\omega_{k_\perp} \tau_0)^2$ when $\omega_{k_\perp} \tau_0 \ll 1$, while the longitudinal components of $\langle \hat{\mathbf{B}}_k \rangle$ and $\langle \hat{\mathbf{E}}_k \rangle$ are independent of $\omega_{k_\perp} \tau_0$ in this limit. Therefore, when $\omega_{k_\perp} \tau_0 \ll 1$, the transverse components are much smaller than the longitudinal components.

We consider two different profiles of the initial macroscopic fields, which are distinguished from each other by different momentum distributions $f(\omega_{k_\perp})$: One $f(\omega_{k_\perp})$ is given by a step function, while the other is given by a difference of Gaussians as adopted in Ref. [63],

$$\text{Type 1 } |f_1(\omega_{k_\perp})|^2 = \Theta(Q_s - \omega_{k_\perp}), \quad (65)$$

$$\text{Type 2 } |f_2(\omega_{k_\perp})|^2 = \frac{Q_s^2}{2\omega_{k_\perp}^2} \left[e^{-k_\perp^2/2Q_s^2} - e^{-k_\perp^2/Q_s^2} \right], \quad (66)$$

where Q_s characterizes the typical transverse momentum. We take Q_s as $Q_s \tau_0 = 0.1 \ll 1$, which implies that the macroscopic color electric and color magnetic fields are parallel to the collision axis.

4.2.1 *Pressure isotropization.* The energy–momentum (EM) tensor is defined as

$$\hat{T}_{\mu\nu}(x) \equiv -g^{\kappa\sigma} \hat{F}_{\mu\kappa}^a(x) \hat{F}_{\nu\sigma}^a(x) + \frac{1}{4} g_{\mu\nu} g^{\alpha\beta} g^{\gamma\omega} \hat{F}_{\alpha\gamma}^a(x) \hat{F}_{\beta\omega}^a(x). \quad (67)$$

To define the pressure and the energy density in the expanding geometry, two types of subtraction are necessary [38],

$$\varepsilon \equiv \frac{1}{V} \sum_x g_{\tau\tau} \langle \hat{T}^{\tau\tau}(x) \rangle_{\text{mac+fluc}} - \frac{1}{V} \sum_x g_{\tau\tau} \langle \hat{T}^{\tau\tau}(x) \rangle_{\text{vac}} - \frac{\alpha}{\tau^2}, \quad (68)$$

$$P_i \equiv \frac{1}{V} \sum_x g_{ii} \langle \hat{T}^{ii}(x) \rangle_{\text{mac+fluc}} - \frac{1}{V} \sum_x g_{ii} \langle \hat{T}^{ii}(x) \rangle_{\text{vac}} - \delta_{i,\eta} \frac{\alpha}{\tau^2}, \quad (69)$$

where $\langle \rangle_{\text{mac+fluc}}$ denotes the average in the test particles with the initial conditions given in Eq. (65) or Eq. (66), $\langle \rangle_{\text{vac}}$ denotes the vacuum contribution, and α/τ^2 is the remaining divergence after subtracting the vacuum contribution; see Appendix B for details.

In actual calculations, the vacuum contribution $\langle \hat{T}^{\mu\mu} \rangle_{\text{vac}}$ is evaluated by the test particle method with vanishing initial macroscopic fields, $\langle \hat{\Phi}_k^{a\lambda} \rangle \Big|_{\tau=\tau_0} = \langle \hat{\Pi}_k^{a\lambda} \rangle \Big|_{\tau=\tau_0} = 0$. Following Ref. [38], the remaining divergent part α/τ^2 is extracted phenomenologically by a fitting procedure as shown in Appendix B.

Figure 2 shows the time evolution of the transverse and longitudinal pressures, P_\perp and P_η , normalized by the energy density ε at $g = 0.1$ and 0.2 for the two types of initial conditions. It is noted that the error bars are large at small $Q_s \tau$ because large subtractions are needed. In the initial stage with $Q_s \tau < (1-2)$, P_η is negative, which reflects that the macroscopic color electric and magnetic fields are parallel to the collision axis in the earliest stage. Then, until $Q_s \tau < (2-3)$, P_\perp and P_η tend to come closer, and there is no g dependence of their values at this period. In the later stage with $Q_s \tau > (2-3)$, P_\perp/ε and P_η/ε gradually approach some different constant values, respectively, with oscillatory behaviors, the amplitudes of which become tiny in the large- $Q_s \tau$ region. The ratio P_η/P_\perp in the final stage clearly deviates from unity; although it slightly gets closer for larger $g (= 0.2)$ the difference between them is still large, which means that isotropization of the pressure is not achieved with $g \leq 0.2$. In a previous study based on the McLerran–Venugopalan model [38], such pressure isotropization was found at $g = 0.5$ and not

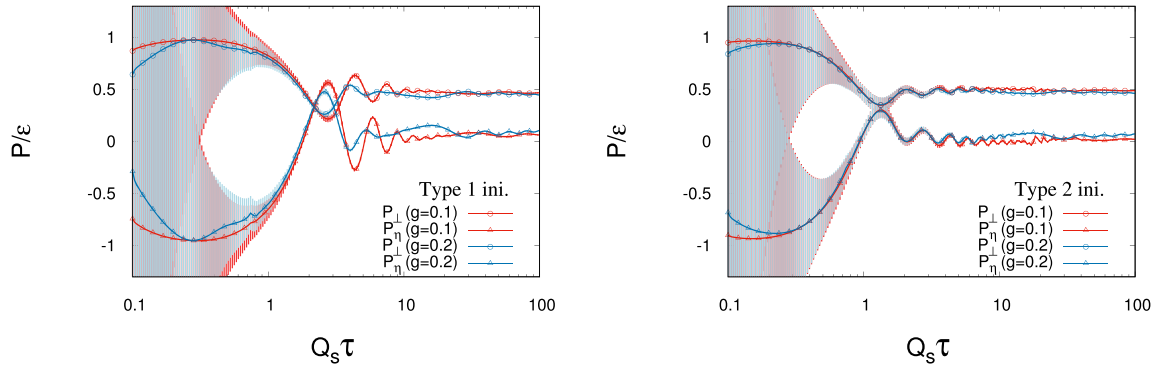


Fig. 2. The time evolution of the transverse and longitudinal pressures, P_{\perp} and P_{η} , per energy density ε of Yang–Mills theory in the expanding geometry on a $32^2 \times 420$ lattice, with $g = 0.1$ and 0.2 ; the smearing parameter σ is set by a constraint $\sigma/g^2 = 1000$. The left and right panels show the results with initial conditions of types 1 and 2, respectively. The number of test particles is $N_{\text{TP}} = 96$. The lines with circles and triangles show P_{\perp}/ε and P_{η}/ε , respectively.

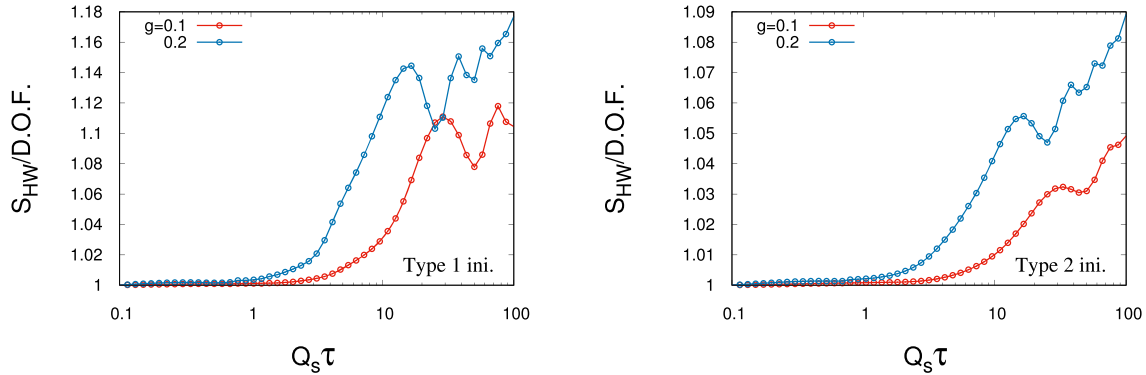


Fig. 3. The time evolution of the HW entropy S_{HW} per degrees of freedom with the initial conditions of type 1 (left) and type 2 (right). The other calculational conditions are the same as in Fig. 2.

at $g = 0.1$. Therefore, our results do not contradict theirs. It is noted that the nearly constant behavior of P_{\perp}/P_{η} at later times shown in Fig. 2 seems consistent with the kinetics results [64]. Such consistency may imply that the semiclassical description and the kinetic description commonly take into account one of the essential processes in the Yang–Mills theory [65,66].

4.2.2 Creation and growth of (Husimi–Wehrl) entropy. In Fig. 3, we show the time evolution of $S_{\text{HW}} = S_{\text{HW}}^{\text{aTP}}$ per degrees of freedom with $g = 0.1$ and 0.2 for the two types of initial conditions. Firstly, we remark that S_{HW} initially agrees with unity with an error of less than 0.01%, which is in accordance with the fact that the initial conditions are prepared as a coherent state. In the earliest stage with $Q_s \tau < (2-3)$, the HW entropy hardly increases, and then in the intermediate stage with $Q_s \tau < (20-30)$, it shows rapid growth. Then it still shows an increase on average but with a smaller growth rate and an oscillatory behavior imposed. For both of the initial conditions, the larger the coupling constant, the larger the growth rate of the HW entropy. In Refs. [39,40], it was shown in the semiclassical simulation with the *non-expanding geometry* that in the last stage where the HW entropy production has been saturated with a small production speed, the Yang–Mills field configuration is already close to that in equilibrium. It

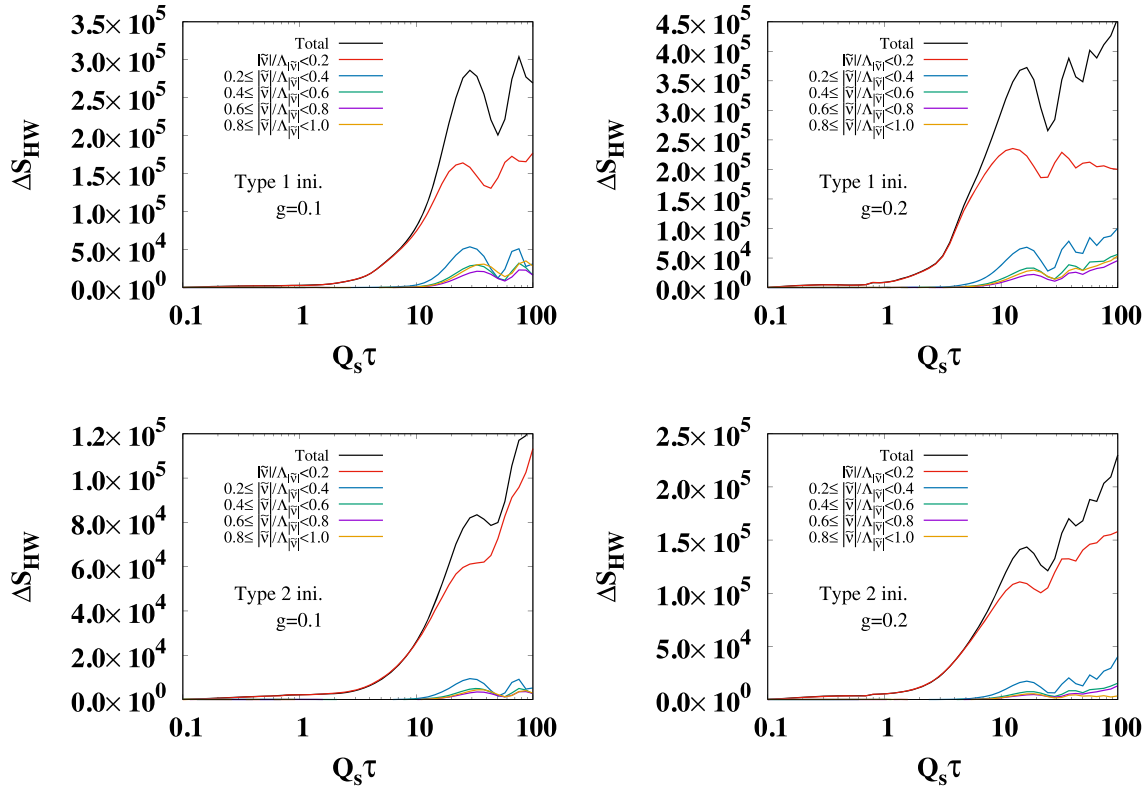


Fig. 4. The HW entropy increase after time evolution, $\Delta S_{\text{HW}} = S_{\text{HW}} - N_{\text{dof}}$, in several longitudinal momentum intervals with $g = 0.1$ and 0.2 for the two types of initial conditions. The bin size in the longitudinal momentum is $|\bar{v}|/\Lambda_{|\bar{v}|} = 0.2$. The left (right) panels show the numerical results with $g = 0.1(0.2)$ and the upper (lower) panels are for the type 1 (type 2) initial conditions.

should be noticed, however, that the similar slow production rate of the HW entropy seen in Fig. 3 does not readily mean that the system is near equilibrium since the large anisotropy of the pressure still remains in the present case with an expanding geometry, which may account for, at least partly, the slow production rate of the entropy, which is actually caused by the fact that the system is still in a nonequilibrium state.

4.2.3 Relationship between particle distribution and Husimi–Wehrl entropy. To understand the underlying mechanism of the HW entropy production, we investigate the time evolution of the particle number as well as the HW entropy *piecewise* with respect to different longitudinal momentum modes with an interval $|\bar{v}|/\Lambda_{|\bar{v}|} = 0.2$, where $\Lambda_{|\bar{v}|}$ denotes the ultraviolet cutoff of the momentum. Figure 4 shows the entropy increase after time evolution $\Delta S_{\text{HW}} = S_{\text{HW}} - N_{\text{dof}}$ in several longitudinal momentum intervals with $g = 0.1$ and 0.2 for the two types of initial conditions. We find that the large HW entropy is first produced in the lowest longitudinal momentum interval, $|\bar{v}|/\Lambda_{|\bar{v}|} < 0.2$, which is followed by a slow increase of the HW entropy in the higher longitudinal momentum intervals. Thus, the rapid production of the HW entropy shown in Fig. 3 occurs in the low longitudinal momentum modes.

To quantify the above observation, we analyze the effective particle numbers, since one of the proposed mechanisms of thermalization is the decay of the Yang–Mills field to particles. We define an effective particle number N_ν as a function of the longitudinal momentum ν integrated

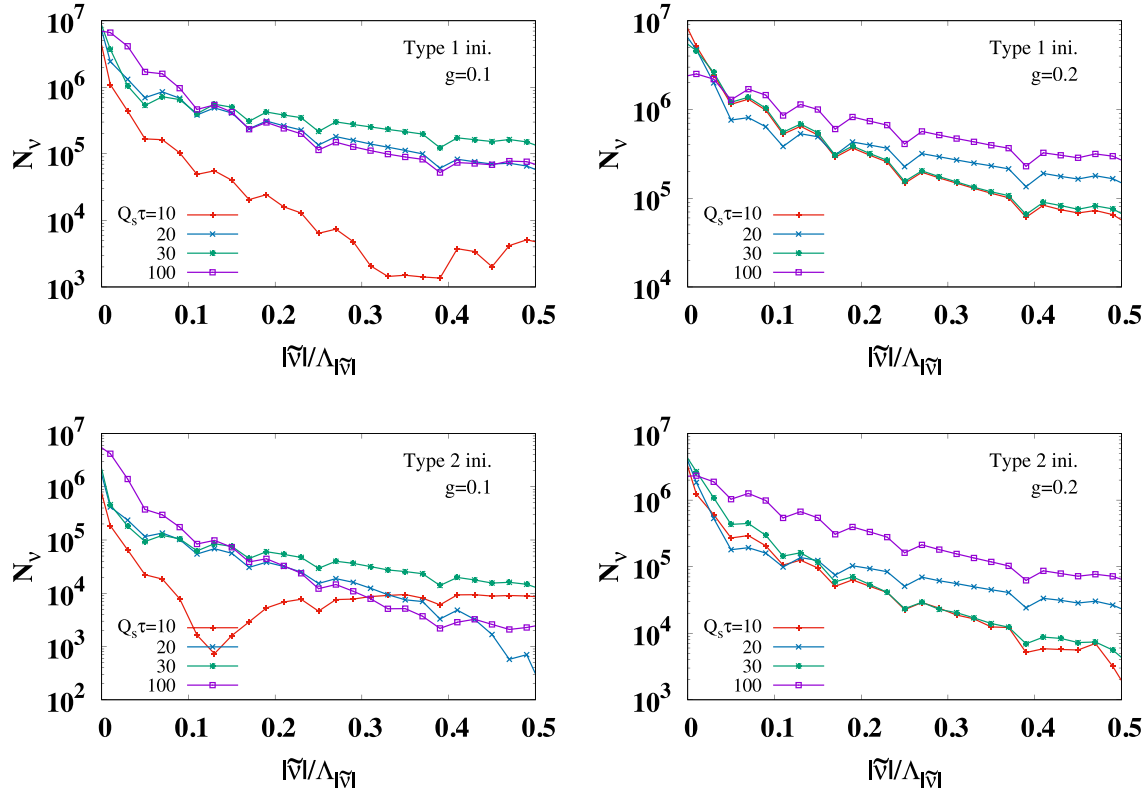


Fig. 5. The time evolution of the effective particle number distribution N_v as a function of the longitudinal momentum \tilde{v} as defined in Eq. (70) with the two initial conditions and coupling constants $g = 0.1$ and 0.2 . The upper-left and upper-right panels show the numerical results for the type 1 initial condition with $g = 0.1$ and 0.2 , respectively, while the lower panels show those for the type 2 initial condition with the same g .

over the transverse momenta as

$$\begin{aligned}
 N_v &\equiv \sum_{k_{\perp, \lambda, a}} \left\{ \left\langle \left(\hat{a}_k^{a\lambda\dagger} - \langle \hat{a}_k^{a\lambda\dagger} \rangle \right) \left(\hat{a}_k^{a\lambda} - \langle \hat{a}_k^{a\lambda} \rangle \right) - \frac{1}{2} \right\rangle \right\} \\
 &= \sum_{k_{\perp, \lambda, a}} \left\{ \langle \hat{a}_k^{a\lambda\dagger} \hat{a}_k^{a\lambda} \rangle - \langle \hat{a}_k^{a\lambda\dagger} \rangle \langle \hat{a}_k^{a\lambda} \rangle - \frac{1}{2} \right\}. \quad (70)
 \end{aligned}$$

Here we regard the creation and annihilation operators subtracted with their expectation values as those operators for the particles under the background classical field. This will be a reasonable description, since the particle number is counted as zero for a coherent state, where the HW entropy takes the minimum value. It should be noted that the last term of $-1/2$ comes from the semiclassical treatment and the uncertainty relation. In a semiclassical treatment, we cannot distinguish the order of the operators and the expectation value of the symmetrized operator (Weyl product) is observed. For example, the expectation value of the number operator $\langle \hat{a}^\dagger \hat{a} \rangle$ is calculated as $\langle (\hat{a}^\dagger \hat{a} + \hat{a} \hat{a}^\dagger)/2 \rangle = \langle (\omega^2 \hat{x}^2 + \hat{p}^2)/(2\omega) \rangle$ for a harmonic oscillator, and its minimum value is $1/2$ as long as the distribution respects the uncertainty principle. Thus a nonzero N_v signals entropy production, when we start from a coherent state initial condition.

In Fig. 5, we show the effective particle number as a function of the longitudinal momentum \tilde{v} at several values of τ . At the initial state, which is set up to be a coherent state, we find $N_v = 0$ (not shown in the figure) as expected. In the earlier stage with $Q_s \tau = 10$ (red curves),

particles with far lower longitudinal momenta dominate over those in other momentum regions. At later times, particles with higher longitudinal momenta start to increase. The early entropy production at lower longitudinal momenta shown before is thus naturally understood to be associated with low momentum particle production.

Comparing Figs. 4 and 5, we find that particle creation is associated with HW entropy production, and there are two distinct stages in the evolution of fields. In the first stage, the particle number in the low longitudinal momentum region grows and the HW entropy from the low longitudinal momentum modes increases rapidly. In the second stage, the effective particle number at higher longitudinal momenta grows and the HW entropy of higher longitudinal momentum modes increases slowly.

5. Summary

We have investigated the possible thermalization process of the highly occupied and weakly coupled Yang–Mills fields in an expanding geometry through a computation of the entropy, as given by the Husimi–Wehrl (HW) entropy, (an)isotropization of the pressure, and the particle production within the semiclassical approximation: The time evolution of the system was obtained by solving the equation of motion of the Wigner function with use of the test particle method; the Husimi function is obtained by smearing the evaluated Wigner function in the phase space. The initial condition of the simulation was constructed so as to mimic the glasma initial condition [9–13], where the macroscopic color electric and color magnetic fields are boost invariant and parallel to the collisional axis. As such, we have considered two types of initial conditions whose momentum distributions are different from each other.

To obtain the HW entropy S_{HW} defined in terms of the Husimi function, it was first calculated by two different test particle methods, one is called the “single test particle method (sTP)” and the other is called the “parallel test particle method (pTP)”. The resultant values thus obtained are denoted by $S_{\text{HW}}^{\text{pTP}}$ and $S_{\text{HW}}^{\text{sTP}}$, respectively, and are shown to satisfy the inequalities $S_{\text{HW}}^{\text{sTP}} < S_{\text{HW}} < S_{\text{HW}}^{\text{pTP}}$. We have shown that the average value of them, $S_{\text{HW}}^{\text{aTP}}$, turns out to give an excellent estimate of S_{HW} with numerical errors of $\mathcal{O}(N_{\text{TP}}^{-2})$ with N_{TP} being the number of test particles, $S_{\text{HW}}^{\text{aTP}} = S_{\text{HW}} + \mathcal{O}(N_{\text{TP}}^{-2})$, while $S_{\text{HW}}^{\text{sTP}}$ and $S_{\text{HW}}^{\text{pTP}}$ have numerical errors of $\mathcal{O}(N_{\text{TP}}^{-1})$, $S_{\text{HW}}^{\text{sTP(pTP)}} = S_{\text{HW}} + \mathcal{O}(N_{\text{TP}}^{-1})$. Nevertheless, to circumvent the computational difficulty in calculating the multiple integration in the HW entropy, we have taken the product ansatz for the Wigner function.

Before proceeding with the study of the Yang–Mills field in the expanding geometry, the above computational method was checked by applying it to the massless ϕ^4 scalar theory in Minkowski spacetime. The numerical results in the scalar theory have indicated that $S_{\text{HW}}^{\text{sTP}} < S_{\text{HW}} < S_{\text{HW}}^{\text{pTP}}$ and $S_{\text{HW}}^{\text{aTP}} \sim S_{\text{HW}}$ nicely hold. It has been found that S_{HW} increases rapidly, then the growth rate becomes moderate, and finally stops increasing and keeps almost a constant value. The saturation of S_{HW} indicates the achievement of equilibration of the system.

We have investigated the dynamical production of the HW entropy in the semiclassical evolution of the Yang–Mills field in the expanding geometry at $g = 0.1$ and 0.2 . We have also shown the semiclassical evolution of the transverse and longitudinal pressures, P_{\perp} and P_{η} . Up to $Q_s\tau < (2-3)$, P_{\perp} and P_{η} have been found to approach each other, and there is no g dependence in this time region. In the later stage with $Q_s\tau > (2-3)$, P_{\perp} and P_{η} have been found to approach some constant values slowly showing oscillatory behavior. The amplitude of the oscillation becomes smaller at large $Q_s\tau$. The longitudinal pressure relative to the transverse pressure, P_{η}/P_{\perp} , has

been found to come slightly closer as g increases, but pressure isotropization was not achieved, which is not in contradiction with a previous work [38] where a much larger coupling constant was used. After the earliest stage with $Q_s\tau < (2-3)$, where the HW entropy in the expanding geometry hardly increases, it grows rapidly in the following time range, $Q_s\tau < (20-30)$, and then increases more slowly in the later stage with $Q_s\tau > (20-30)$. For both types of initial conditions, the growth rate of the HW entropy at $g = 0.2$ is larger than that at $g = 0.1$. The slow HW entropy production stage does not readily mean that the system is near equilibrium since the large anisotropy of the pressure still remains in our simulations. Such a slow production far from equilibrium is expected to be caused by the longitudinal expansion effect.

We have defined the effective particle number so that it represents the particle number created due to the deviations from the coherent state and have compared its time evolution and the time evolution of the HW entropy piecewise with respect to the longitudinal momentum mode. We have found that the effective particle number and the HW entropy production are associated with each other, and there are two distinct time stages in the time evolution of the Yang–Mills fields: In the first stage, the particle number distribution in the low longitudinal momentum region grows and the HW entropy of the longitudinal low momentum modes increases rapidly, while in the second stage the particle number distribution at higher longitudinal momentum grows and the HW entropy of corresponding modes increases slowly.

Since our choice of the initial conditions only mimics the glasma state, we should directly take the McLerran–Venugopalan model in order to make the model more realistic [13]. It is also a rather urgent subject to perform calculations at larger coupling constants such as $g = 0.5$, which is used in the previous calculation [38], thereby clarifying the coupling dependence of the way of the thermalization process.

Acknowledgements

This work is supported in part by Grants-in-Aid for Scientific Research from the Japan Society for the Promotion of Science (JSPS) (Nos. 19K03872, 19H01898, 19H05151, and 21H00121) and by the Yukawa International Program for Quark–Hadron Sciences (YIPQS).

Funding

Open Access funding: SCOAP³.

Appendix A. Second quantization of a free gauge field in an expanding geometry

In this appendix, we present the second-quantized formulation of a free gauge field in the τ – η coordinate, which is found convenient to analyze fluctuations in the expanding glasma [42,62,67]. This appendix refers to Ref. [42].

First, we begin by showing the way of the second quantization in the continuum limit. In this paragraph only, none of the quantities are normalized by lattice spacings. The equation of motion for the free gauge field $[D, F] = 0$ describing the τ evolution reads

$$\partial_1 \partial_\tau A_1(x) + \partial_2 \partial_\tau A_2(x) + \frac{1}{\tau^2} \partial_\eta \partial_\tau A_\eta(x) = 0, \quad (\text{A1})$$

$$\left(\partial_\tau^2 + \frac{1}{\tau} \partial_\tau - \partial_1^2 - \partial_2^2 - \frac{\partial_\eta^2}{\tau^2} \right) A_i(x) + \partial_i \left(\partial_1 A_1(x) + \partial_2 A_2(x) + \frac{1}{\tau^2} \partial_\eta A_\eta(x) \right) = 0, \quad (\text{A2})$$

$$\left(\partial_\tau^2 - \frac{1}{\tau}\partial_\tau - \partial_1^2 - \partial_2^2 - \frac{\partial_\eta^2}{\tau^2}\right)A_\eta(x) + \partial_\eta\left(\partial_1 A_1(x) + \partial_2 A_2(x) + \frac{1}{\tau^2}\partial_\eta A_\eta(x)\right) = 0. \quad (\text{A3})$$

For the Fourier modes with finite transverse momentum mode, the general solution satisfying the Coulomb type gauge condition, $(\partial_1 A_1 + \partial_2 A_2 + \tau^{-2}\partial_\eta A_\eta)|_{\tau=\tau_0} = 0$, is expressed in terms of the Hankel function,

$$A_\mu = \sum_{\lambda=1,2} \int \frac{d^3\mathbf{k}}{(2\pi)^3} \left(\xi_k^{\lambda,(1)} \mathcal{A}_{\mu,k}^{(-)\lambda}(\tau) e^{i(\mathbf{k}_\perp \cdot \mathbf{x}_\perp + \nu\eta)} + \xi_k^{\lambda,(2)} \mathcal{A}_{\mu,k}^{(+)\lambda}(\tau) e^{i(\mathbf{k}_\perp \cdot \mathbf{x}_\perp + \nu\eta)} \right), \quad (\text{A4})$$

$$\mathcal{A}_{\mu,k}^{(-/+)\lambda}(\tau) = \frac{i}{k_\perp} (0, k_2, -k_1, 0) H_{iv}^{(1/2)}(k_\perp \tau), \quad (\text{A5})$$

$$\mathcal{A}_{\mu,k}^{(+/-)2}(\tau) = -\frac{\nu}{k_\perp} \left(0, k_1 \alpha_{iv}^{(1/2)}(k_\perp \tau), k_2 \alpha_{iv}^{(1/2)}(k_\perp \tau), -\frac{1}{\nu} \beta_{iv}^{(1/2)}(k_\perp \tau) \right), \quad (\text{A6})$$

$$\alpha_{iv}^{(1/2)}(k_\perp \tau) = \int_{k_\perp \tau_0}^{k_\perp \tau} dz \frac{1}{z} H_{iv}^{(1/2)}(z) - \frac{k_\perp \tau_0}{\nu^2 + (k_\perp \tau_0)^2} \dot{H}_{iv}^{(1/2)}(k_\perp \tau_0), \quad (\text{A7})$$

$$\beta_{iv}^{(1/2)}(k_\perp \tau) = \int_{k_\perp \tau_0}^{k_\perp \tau} dz z H_{iv}^{(1/2)}(z) - \frac{(k_\perp \tau_0)^3}{\nu^2 + (k_\perp \tau_0)^2} \dot{H}_{iv}^{(1/2)}(k_\perp \tau_0), \quad (\text{A8})$$

where $k_\perp = \sqrt{k_1^2 + k_2^2}$ is a transverse momentum and $\xi_k^{\lambda,i}$ is a given constant. The solution, $\mathcal{A}_{\mu,k}^{(i)\lambda}(\tau) e^{i(\mathbf{k}_\perp \cdot \mathbf{x}_\perp + \nu\eta)}$, is orthogonal to other solutions with different indexes $(\lambda', i', \mathbf{k}') \neq (\lambda, i, \mathbf{k})$,

$$\left(\mathcal{A}_{\mu,k}^{(i)\lambda}(\tau) e^{i\mathbf{k} \cdot \mathbf{x}}, \mathcal{A}_{\mu',k'}^{(i')\lambda'}(\tau) e^{i\mathbf{k}' \cdot \mathbf{x}} \right) = 0, \quad (\text{A9})$$

with respect to a scalar product defined as

$$(f_\mu(x), g_\mu(x)) = -i \int d^3\mathbf{x} \tau g^{\mu\nu} (f_\mu^*(x) \partial_\tau g_\nu(x) - g_\nu(x) \partial_\tau f_\mu^*(x)). \quad (\text{A10})$$

If $(\lambda', i', \mathbf{k}') = (\lambda, i, \mathbf{k})$, the scalar product does not vanish and is invariant under the τ evolution according to Eqs. (A1)–(A3). Since the second kind of Hankel function asymptotically behaves as the positive frequency mode,

$$H_{iv}^{(i)}(k_\perp \tau) \rightarrow \sqrt{\frac{2}{\pi k_\perp \tau}} \exp\left[-i\left(k_\perp \tau - \frac{\pi}{4}\right) - \frac{\pi\nu}{2}\right] \quad (k_\perp \tau \rightarrow \infty), \quad (\text{A11})$$

we can obtain the expression of the second-quantized gauge field as a linear combination of $\mathcal{A}_{\mu,k}^{(+)\lambda}(\tau, \mathbf{k})$ and $\mathcal{A}_{\mu,k}^{(+)\lambda'}(\tau, \mathbf{k})$,

$$A_i(x) = \sum_\lambda \int \frac{d^3\mathbf{k}}{(2\pi)^3} \left(\hat{a}_k^\lambda \mathcal{A}_{\mu,k}^\lambda(\tau) e^{i(\mathbf{k}_\perp \cdot \mathbf{x}_\perp + \nu\eta)} + \text{h.c.} \right), \quad (\text{A12})$$

$$\mathcal{A}_{\mu,k}^\lambda(\tau) = \sqrt{\frac{\pi}{4}} e^{\frac{\pi|\nu|}{2}} \mathcal{A}_{\mu,k}^{(+)\lambda}(\tau), \quad (\text{A13})$$

$$[\hat{a}_k^\lambda, \hat{a}_{k'}^{\lambda'\dagger}] = (2\pi)^3 \delta_{\lambda,\lambda'} \delta(\mathbf{k} - \mathbf{k}'). \quad (\text{A14})$$

Here we determine the normalization constant in front of $\mathcal{A}_{\mu,k}^{(+)\lambda}(\tau)$ in Eq. (A13) so as to satisfy the orthonormal condition,

$$\begin{aligned} & \left(\sqrt{\frac{\pi}{4}} e^{\frac{\pi|\nu|}{2}} \mathcal{A}_{\mu,k}^{(+)\lambda}(\tau) e^{i(\mathbf{k}_\perp \cdot \mathbf{x}_\perp + \nu\eta)}, \sqrt{\frac{\pi}{4}} e^{\frac{\pi|\nu'|}{2}} \mathcal{A}_{\mu,k'_\perp,\nu'}^{(+)\lambda'}(\tau) e^{i(\mathbf{k}'_\perp \cdot \mathbf{x}_\perp + \nu'\eta)} \right) \\ &= (2\pi)^3 \delta_{\lambda,\lambda'} \delta(\mathbf{k}_\perp - \mathbf{k}'_\perp) \delta(\nu - \nu'). \end{aligned} \quad (\text{A15})$$

The procedure of the second quantization using such a scalar product is standard in quantum field theory in curved spacetime. In our analysis, we only treat the finite transverse momentum modes since the contribution of the 0 transverse mode decreases as the transverse size of the system increases.

Next, we show the second quantization of the free gauge field on a space lattice with continuous time. The equation of motion reads

$$\partial_1^B \partial_\tau A_1(x) + \partial_2^B \partial_\tau A_2(x) + \frac{1}{a_\eta^2 \tau^2} \partial_\eta^B \partial_\tau A_\eta(x) = 0, \quad (\text{A16})$$

$$\left(\partial_\tau^2 + \frac{1}{\tau} \partial_\tau - \partial_1^B \partial_1^F - \partial_2^B \partial_2^F - \frac{\partial_\eta^B \partial_\eta^F}{a_\eta^2 \tau^2} \right) A_i(x) + \partial_i \left(\partial_1^B A_1(x) + \partial_2^B A_2(x) + \frac{1}{a_\eta^2 \tau^2} \partial_\eta^B A_\eta(x) \right) = 0, \quad (\text{A17})$$

$$\left(\partial_\tau^2 - \frac{1}{\tau} \partial_\tau - \partial_1^B \partial_1^F - \partial_2^B \partial_2^F - \frac{\partial_\eta^B \partial_\eta^F}{a_\eta^2 \tau^2} \right) A_\eta(x) + \partial_i \left(\partial_1^B A_1(x) + \partial_2^B A_2(x) + \frac{1}{a_\eta^2 \tau^2} \partial_\eta^B A_\eta(x) \right) = 0, \quad (\text{A18})$$

where ∂_i^B denotes a backward difference operator in the i -direction. In much the same way as the continuum case, we can get the expression of the second-quantized gauge field as

$$A_i(x) = \frac{1}{\sqrt{L_\perp^2 L_\eta}} \sum_{\lambda, k} \left(\hat{a}_k^\lambda \tilde{A}_{\mu, k}^\lambda(\tau) e^{i(\mathbf{k}_\perp \cdot \mathbf{x}_\perp + \nu \eta)} + \text{h.c.} \right), \quad (\text{A19})$$

$$\left[\hat{a}_k^\lambda, \hat{a}_k^{\lambda' \dagger} \right] = \delta_{\lambda, \lambda'} \delta_{k, k'}, \quad (\text{A20})$$

$$\tilde{A}_{\mu, k}^1(\tau) = \frac{i}{\omega_{\mathbf{k}_\perp}} \sqrt{\frac{\pi}{4a_\eta}} e^{\frac{\pi i |\tilde{\nu}|}{2a_\eta}} (0, \tilde{k}_2, \tilde{k}_1, 0) H_{i|\tilde{\nu}|/a_\eta}^{(2)}(\omega_{\mathbf{k}_\perp} \tau), \quad (\text{A21})$$

$$\tilde{A}_{\mu, k}^2(\tau) = -\frac{\tilde{\nu}^*}{a_\eta \omega_{\mathbf{k}_\perp}} \sqrt{\frac{\pi}{4a_\eta}} e^{\frac{\pi i |\tilde{\nu}|}{2a_\eta}} \left(0, \tilde{k}_1 \alpha_{i|\tilde{\nu}|/a_\eta}^{(2)}(\omega_{\mathbf{k}_\perp} \tau), \tilde{k}_2 \alpha_{i|\tilde{\nu}|/a_\eta}^{(2)}(\omega_{\mathbf{k}_\perp} \tau), -\frac{a_\eta^2}{\tilde{\nu}^*} \beta_{i|\tilde{\nu}|/a_\eta}^{(2)}(\omega_{\mathbf{k}_\perp} \tau) \right). \quad (\text{A22})$$

By utilizing this expression, the electric field and the free part of the magnetic field are also written in terms of the annihilation and creation operators,

$$\hat{E}^i(x) = \frac{1}{\sqrt{L_\perp^2 L_\eta}} \sum_{\lambda, k} \left(\hat{a}_k^\lambda \mathcal{E}_k^{\lambda, i}(\tau) e^{i(\mathbf{k}_\perp \cdot \mathbf{x}_\perp + \nu \eta)} + \text{h.c.} \right), \quad (\text{A23})$$

$$\hat{B}_0^i(x) = \frac{1}{2} \varepsilon^{ijk} \partial_j^F A_k(x) = \frac{1}{\sqrt{L_\perp^2 L_\eta}} \sum_{\lambda, k} \left(\hat{a}_k^\lambda \mathcal{B}_k^{\lambda, i}(\tau) e^{i(\mathbf{k}_\perp \cdot \mathbf{x}_\perp + \nu \eta)} + \text{h.c.} \right), \quad (\text{A24})$$

$$\mathcal{E}_k^{1, i}(\tau) = \dot{H}_{i|\tilde{\nu}|/a_\eta}^{(2)}(\omega_{\mathbf{k}_\perp} \tau) \varepsilon_k^{1, i}, \quad \mathcal{E}_k^{2, i}(\tau) = H_{i|\tilde{\nu}|/a_\eta}^{(2)}(\omega_{\mathbf{k}_\perp} \tau) \varepsilon_k^{2, i}, \quad (\text{A25})$$

$$\mathcal{B}_k^{1, i}(\tau) = H_{i|\tilde{\nu}|/a_\eta}^{(2)}(\omega_{\mathbf{k}_\perp} \tau) \varepsilon_k^{2, i*}, \quad \mathcal{B}_k^{2, i}(\tau) = \dot{H}_{i|\tilde{\nu}|/a_\eta}^{(2)}(\omega_{\mathbf{k}_\perp} \tau) \varepsilon_k^{1, i*}, \quad (\text{A26})$$

$$\varepsilon_k^{1, i} = ia_\eta \tau \sqrt{\frac{\pi}{4a_\eta}} e^{\frac{\pi i |\tilde{\nu}|}{2a_\eta}} (\tilde{k}_2^*, -\tilde{k}_1^*, 0), \quad \varepsilon_k^{2, i} = -\frac{\tilde{\nu}^*}{\omega_{\mathbf{k}_\perp}} \sqrt{\frac{\pi}{4a_\eta}} e^{\frac{\pi i |\tilde{\nu}|}{2a_\eta}} \left(\tilde{k}_1, \tilde{k}_2, -\frac{\omega_{\mathbf{k}_\perp}^2}{\tilde{\nu}^*} \right). \quad (\text{A27})$$

Solving Eqs. (A23) and (A24) with respect to \hat{a}_k^λ , we can write \hat{a}_k^λ as a linear combination of the Fourier modes (\hat{E}_k, \hat{B}_k) ,

$$\hat{a}_k^1 = \frac{i}{a_\eta \omega_{k_\perp} \tau} \times \left(\frac{\omega_{k_\perp}^2}{\omega_{k_\perp}^2 + |\tilde{v}/(\tau a_\eta)|^2} \frac{\dot{H}_{i|\tilde{v}|/a_\eta}^{(2)*}(\omega_{k_\perp} \tau)}{H_{i|\tilde{v}|/a_\eta}^{(2)*}(\omega_{k_\perp} \tau)} [\mathcal{B}_k^{1*} \cdot B_{0,k}(\tau)] + \frac{H_{i|\tilde{v}|/a_\eta}^{(2)*}(\omega_{k_\perp} \tau)}{\dot{H}_{i|\tilde{v}|/a_\eta}^{(2)*}(\omega_{k_\perp} \tau)} [\mathcal{E}_k^{1,*} \cdot E_k(\tau)] \right), \quad (\text{A28})$$

$$\hat{a}_k^2 = \frac{i}{a_\eta \omega_{k_\perp} \tau} \times \left(\frac{\omega_{k_\perp}^2}{\omega_{k_\perp}^2 + |\tilde{v}/(\tau a_\eta)|^2} \frac{\dot{H}_{i|\tilde{v}|/a_\eta}^{(2)*}(\omega_{k_\perp} \tau)}{H_{i|\tilde{v}|/a_\eta}^{(2)*}(\omega_{k_\perp} \tau)} [\mathcal{E}_k^{2*} \cdot E_k(\tau)] + \frac{H_{i|\tilde{v}|/a_\eta}^{(2)*}(\omega_{k_\perp} \tau)}{\dot{H}_{i|\tilde{v}|/a_\eta}^{(2)*}(\omega_{k_\perp} \tau)} [\mathcal{B}_k^{2*} \cdot B_{0,k}(\tau)] \right). \quad (\text{A29})$$

In actual calculations, we use these relations to transform (A, E) to (Φ, Π) through Eqs. (54) and (55).

Appendix B. Divergence in pressure and energy density

In this appendix, we show the remaining divergences in the pressure and energy density after subtracting the vacuum contribution, and discuss how to subtract them. For convenience, we use the following notation, $(\)_{\text{ini mac}}$, which means the contribution of the macroscopic field part of the initial Wigner function to a given observable at the initial time τ_0 . For example, in the case of the Fourier transforms of the color electric and color magnetic fields, $(\mathbf{E}_k^a)_{\text{ini mac}}$ and $(\mathbf{B}_k^a)_{\text{ini mac}}$ have already been given in Eqs. (59)–(64). Thus, the macroscopic field contribution to the initial pressure is given by

$$\begin{aligned} (P_\eta)_{\text{ini mac}} &\sim -(P_\perp)_{\text{ini mac}} = -\frac{1}{V} \sum_x g_{ii} \langle \hat{T}^{ii}(x) \rangle_{\text{ini mac}} \\ &= -\frac{a_\eta \tau}{2} \sum_{a, x_\perp, \eta} [(\hat{E}^{a\eta}(x)^2)_{\text{ini mac}} + (\hat{B}^{a\eta}(x)^2)_{\text{ini mac}}] \\ &\sim -\frac{\Delta}{8L_\perp^2 \alpha_s} \sum_{k_\perp} \omega_{k_\perp}^2 |f_i(\mathbf{k}_\perp)|^2. \end{aligned} \quad (\text{B1})$$

In Fig. 6, we show the $Q_s \tau_0$ dependence of the initial pressure after subtracting the vacuum contribution and the macroscopic field contribution,

$$\tilde{P}_i = \frac{1}{V} \sum_x g_{ii} \langle \hat{T}^{ii}(x) \rangle_{\text{mat+flu}} - \frac{1}{V} \sum_x g_{ii} \langle \hat{T}^{ii}(x) \rangle_{\text{vac}} - (P_i)_{\text{ini mac}}, \quad (\text{B2})$$

normalized by $(P_i)_{\text{ini mac}}$ at $g = 0.1$ and 0.2 for the two types of initial conditions. We find that $|\tilde{P}_\eta / (P_\eta)_{\text{ini mac}}|$ diverges as $(Q_s \tau_0)^{-2}$ since the $Q_s \tau_0$ dependence of $|\tilde{P}_\eta / (P_\eta)_{\text{ini mac}}|$ is reproduced well by the fitting function $f_{\text{pow}}(Q_s \tau_0) = A_{\text{pow}} / (Q_s \tau_0)^2$. We also find that $|\tilde{P}_\perp / (P_\perp)_{\text{ini mac}}|$ diverges as $\ln^2 Q_s \tau_0$ since the $|\tilde{P}_\perp / (P_\perp)_{\text{ini mac}}|$ data lie on the fitting curve $f_{\text{log}}(Q_s \tau_0) = B_{\text{log}} \ln^2(Q_s \tau_0) + C_{\text{log}}$.

Here, we briefly explain how to remove the remaining divergence at any τ based on the method presented in Ref. [38]. As seen above, the remaining divergence in P_\perp at $\tau = \tau_0$ is a logarithmic

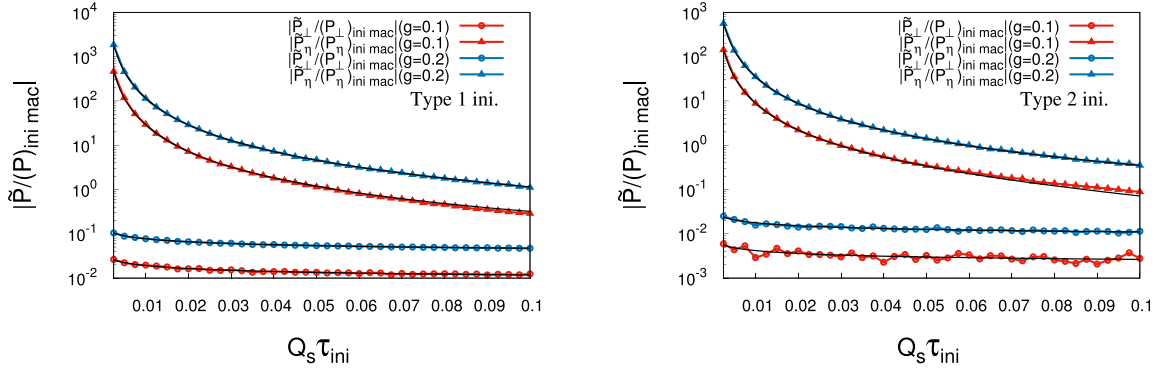


Fig. B1. The $Q_s\tau_0$ dependence of the initial pressure after subtracting the vacuum contribution and the macroscopic field contribution, $\tilde{P}_i = \frac{1}{V} \sum_x g_{ii} \langle \hat{T}^{ii}(x) \rangle_{\text{mat+flu}} - \frac{1}{V} \sum_x g_{ii} \langle \hat{T}^{ii}(x) \rangle_{\text{vac}} - (P_i)_{\text{ini mac}}$, normalized by $(P_i)_{\text{ini mac}}$. These calculations are performed at $g = 0.1$ and 0.2 for the two types of initial conditions. The red (blue) line with circles shows the transverse pressure at $g = 0.1(0.2)$. The red (blue) line with triangular points shows the longitudinal pressure at $g = 0.1(0.2)$. The result in the left (right) panel is calculated with the type 1 (2) initial condition.

function of τ_0 and is much smaller than the initial macroscopic field contribution,

$$B_{\log} \ln^2(Q_s\tau_0) \gg |(P_{\perp})_{\text{ini mac}}|. \quad (\text{B3})$$

Thus, we neglect the remaining divergence in P_{\perp} at any τ . Then we can define the subtracted energy density and pressure as

$$\varepsilon \equiv \frac{1}{V} \sum_x g_{\tau\tau} \langle \hat{T}^{\tau\tau}(x) \rangle_{\text{mac+fluc}} - \frac{1}{V} \sum_x g_{\tau\tau} \langle \hat{T}^{\tau\tau}(x) \rangle_{\text{vac}} - \alpha_{\text{div}}(t), \quad (\text{B4})$$

$$P_i \equiv \frac{1}{V} \sum_x g_{ii} \langle \hat{T}^{ii}(x) \rangle_{\text{mac+fluc}} - \frac{1}{V} \sum_x g_{ii} \langle \hat{T}^{ii}(x) \rangle_{\text{vac}} - \delta_{i,\eta} \alpha_{\text{div}}(t), \quad (\text{B5})$$

where $\alpha_{\text{div}}(\tau)$ represents the divergence that should be removed. The energy density also has the remaining divergence because of the relation between the energy density and pressure, $\varepsilon = P_1 + P_2 + P_{\eta}$. By using the conservation law in the boost-invariant longitudinal (Bjorken) expanding geometry, $\partial\varepsilon/\partial\tau = -\varepsilon + P_{\eta}/\tau$, we obtain the evolution equation for α ,

$$\frac{d\alpha_{\text{div}}}{d\tau} = -\frac{2\alpha_{\text{div}}}{\tau}. \quad (\text{B6})$$

By solving the differential equation, we find $\alpha_{\text{div}}(\tau) = \alpha/\tau^2$, where α is a constant. As seen above, we can obtain $\alpha(\tau_0)$ as $\alpha(\tau_0) = A_{\text{pow}}/(Q_s\tau_0)^2$ by the fit. Thus, we use $\alpha = A_{\text{pow}}$ in the actual calculations.

Appendix C. Evaluation by test particle methods

An integral I consisting of a function $H(\Gamma)$ that is evaluated by test particle methods is expressed as

$$I = \int d\Gamma \mathcal{F}(H(\Gamma)), \quad (\text{C1})$$

where Γ denotes the phase space point under consideration. In general, $H(\Gamma)$ evaluated with the i th set of test particles, which is represented as $H_i(\Gamma)$, has numerical errors $dH_i(\Gamma)$ depending on the phase space point Γ as

$$H_i(\Gamma) = H(\Gamma) + dH_i(\Gamma). \quad (\text{C2})$$

Note that each $H(\Gamma)$ that enters the integral I can be evaluated with different and independent sets of test particles. (When all the test particle sets are identical, it is called the single test particle method.) Then, under the condition $\frac{dH}{H} \ll 1$, the integral I can be expanded as a series of $dH_i(\Gamma)$,

$$I = \int d\Gamma \mathcal{F}(H) + \sum_{i_1, i_2, \dots, i_N} \int d\Gamma \mathcal{F}'_{i_1, i_2, \dots, i_N} dH_1^{i_1} dH_2^{i_2}, \dots, dH_N^{i_N}, \quad (\text{C3})$$

where \mathcal{F}' denotes coefficients in the expansion, and Γ in the functions are omitted. We here consider the situation where the integrals of the odd-order terms of dH disappear due to numerical error cancellation as $\int d\Gamma dH_i^{2n+1}(\Gamma) \mathcal{G}(\Gamma) = 0$, which would be justified when positive and negative contributions of $dH_i(\Gamma)$ equally enter in the integration as $\int d\Gamma dH_i(\Gamma) = 0$ and \mathcal{G} is smooth enough. In such a case, only even-order terms contribute to I 's numerical errors as

$$I = \int d\Gamma \mathcal{F}(H) + \sum_{i_1, i_2, \dots, i_N \in \text{even}} \int d\Gamma \mathcal{F}'_{i_1, i_2, \dots, i_N} dH_1^{i_1} dH_2^{i_2} \dots dH_N^{i_N}, \quad (\text{C4})$$

and the number of terms is greatly reduced.

Let us proceed with the evaluation of an HW entropy based on test particle methods. An HW entropy S can be expressed as

$$S = - \int d\Gamma H(\Gamma) \ln H(\Gamma), \quad (\text{C5})$$

with a Husimi function $H(\Gamma)$. With the parallel test particle (pTP) method in mind, S can be written as

$$\begin{aligned} S &= - \int d\Gamma H_1(\Gamma) \ln H_2(\Gamma) \\ &= - \int d\Gamma (H(\Gamma) + dH_1(\Gamma)) \ln(H(\Gamma) + dH_2(\Gamma)), \end{aligned} \quad (\text{C6})$$

which is further expanded as

$$\begin{aligned} S &= - \int d\Gamma H(\Gamma) \ln H(\Gamma) - \int d\Gamma dH_1(\Gamma) \ln H(\Gamma) - \int d\Gamma dH_2(\Gamma) \\ &\quad - \int d\Gamma \frac{dH_1(\Gamma) dH_2(\Gamma)}{H(\Gamma)} + \int d\Gamma \frac{dH_2^2(\Gamma)}{2H(\Gamma)} + \int d\Gamma \frac{dH_1(\Gamma) dH_2^2(\Gamma)}{2H(\Gamma)} + \dots, \end{aligned} \quad (\text{C7})$$

when $\frac{dH}{H} \ll 1$. In the case where $H(\Gamma)$ is a Husimi function, we have confirmed that the equality $\int d\Gamma H(\Gamma) = 1$ numerically holds with good accuracy, which indicates that positive and negative contributions of $dH_i(\Gamma)$ equally enter in the integration, and the integrals of the odd-order terms of dH are expected to disappear due to numerical error cancellation as $\int d\Gamma dH^{2n+1}(\Gamma) \mathcal{G}(\Gamma) = 0$, since $\mathcal{G}(\Gamma)$ is a function of $H(\Gamma)$, which is a smooth Gaussian-smearred function. Such error cancellation has been numerically confirmed at least in the calculations presented in this paper, and we can leave only even-order terms of dH .

For the single test particle (sTP) method, the errors in and outside the logarithmic function are identical ($dH_1 = dH_2$) and S leads to the form

$$S^{\text{sTP}} = - \int d\Gamma H(\Gamma) \ln H(\Gamma) - \int d\Gamma \frac{dH_2^2(\Gamma)}{2H(\Gamma)}. \quad (\text{C8})$$

For the parallel test particle (pTP) method, dH_1 and dH_2 are independent and

$$S^{\text{pTP}} = - \int d\Gamma H(\Gamma) \ln H(\Gamma) + \int d\Gamma \frac{dH_2^2(\Gamma)}{2H(\Gamma)} \quad (\text{C9})$$

holds. We finally obtain the inequality

$$S^{\text{sTP}} < S < S^{\text{pTP}}. \quad (\text{C10})$$

When the test particles used for evaluating $\ln H(\Gamma)$ are common in sTP and pTP methods, the entropy evaluated with $N_{\text{TP}} \rightarrow \infty$ can be obtained as

$$S = \frac{S^{\text{sTP}} + S^{\text{pTP}}}{2} + \mathcal{O}(N_{\text{TP}}^{-2}), \quad (\text{C11})$$

where we make the reasonable assumption that $dH \propto 1/\sqrt{N_{\text{TP}}}$.

Appendix D. Choice of the smearing parameter

Here we show how the HW entropy defined in Eq. (20), in which the smear parameters are set to the eigenfrequencies, behaves for the Gibbs state and vacuum state of the free field.

We first discuss the HW entropy defined in Eq. (20) for the Gibbs ensemble of the free field, $\rho_{\text{Gibbs}}^{\text{free}} \propto e^{-H_{\text{free}}/T}$. In this case, the total density matrix, $\rho_{\text{Gibbs}}^{\text{free}}$, can be written as the product of the Gibbs ensembles of 1D harmonic oscillators, $\rho_{\text{Gibbs}}^{\text{free}} = \prod_k \rho_{\text{Gibbs},k}^{\text{h.o.}} \propto \prod_k e^{-H_k^{\text{h.o.}}/T}$. Then the total Husimi function can also be written as the product of the Husimi functions for each degree of freedom,

$$f_{\text{H}}(\{\Phi, \Pi, \omega\}) \Big|_{\rho=\rho_{\text{Gibbs}}^{\text{free}}} = \prod_k f_{\text{H}}(\Phi_k, \Pi_k, \omega_k) \Big|_{\rho=\rho_{\text{Gibbs},k}^{\text{h.o.}}}. \quad (\text{D1})$$

Therefore, the total HW entropy, $S_{\text{HW}} \Big|_{\rho=\rho_{\text{Gibbs}}^{\text{free}}}$, is given by the sum of the HW entropy for each degree of freedom,

$$\begin{aligned} S_{\text{HW}}(\{\omega\}) \Big|_{\rho=\rho_{\text{Gibbs}}^{\text{free}}} &= - \int \mathcal{D}\Gamma f_{\text{H}}(\{\Phi, \Pi, \omega\}) \ln f_{\text{H}}(\{\Phi, \Pi, \omega\}) \Big|_{\rho=\rho_{\text{Gibbs}}^{\text{free}}} \\ &= \sum_k - \int \frac{d\Phi_k d\Pi_k}{2\pi} f_{\text{H}}(\Phi_k, \Pi_k, \omega_k) \ln f_{\text{H}}(\Phi_k, \Pi_k, \omega_k) \Big|_{\rho=\rho_{\text{Gibbs},k}^{\text{h.o.}}} \\ &= \sum_k S_{\text{HW}}(\omega_k) \Big|_{\rho=\rho_{\text{Gibbs},k}^{\text{h.o.}}}. \end{aligned} \quad (\text{D2})$$

On the basis of the discussion of the HW entropy of a 1D harmonic oscillator with the smearing parameter being set to its eigenfrequency, which is given in Sect. 5 in Ref. [49], the HW entropy for each degree of freedom, $S_{\text{HW}}(\omega_k) \Big|_{\rho=\rho_{\text{Gibbs},k}^{\text{h.o.}}}$, is found to be larger than the von Neumann entropy $S_{\text{vN}} (= -\text{Tr}(\rho_{\text{Gibbs},k}^{\text{h.o.}} \ln \rho_{\text{Gibbs},k}^{\text{h.o.}}))$ obtained from the same density matrix, but to agree with it in the high-temperature limit,

$$S_{\text{HW}}(\omega_k) \Big|_{\rho=\rho_{\text{Gibbs},k}^{\text{h.o.}}} > S_{\text{vN}} \Big|_{\rho=\rho_{\text{Gibbs},k}^{\text{h.o.}}}, \quad (\text{D3})$$

$$\lim_{T \rightarrow \infty} S_{\text{HW}}(\omega_k) \Big|_{\rho=\rho_{\text{Gibbs},k}^{\text{h.o.}}} = \lim_{T \rightarrow \infty} S_{\text{vN}} \Big|_{\rho=\rho_{\text{Gibbs},k}^{\text{h.o.}}}. \quad (\text{D4})$$

Accordingly, the same relationship holds for the total HW entropy and the von Neumann entropy given as a sum of harmonic oscillators,

$$S_{\text{HW}}(\{\omega\}) \Big|_{\rho=\rho_k^{\text{free}}} > S_{\text{vN}} \Big|_{\rho=\rho_k^{\text{free}}}, \quad (\text{D5})$$

$$\lim_{T \rightarrow \infty} S_{\text{HW}}(\{\omega\}) \Big|_{\rho=\rho_k^{\text{free}}} = \lim_{T \rightarrow \infty} S_{\text{vN}} \Big|_{\rho=\rho_k^{\text{free}}}, \quad (\text{D6})$$

where $S_{\text{vN}}\Big|_{\rho=\rho_k^{\text{free}}} = \sum_k S_{\text{vN}}\Big|_{\rho=\rho_{\text{Gibbs},k}^{\text{h.o.}}}$. This shows that the HW entropy $S_{\text{HW}}(\{\omega_k\})$ adopted in our study agrees with the von Neumann entropy in the high-temperature and weak-coupling limit.

Next, we show that the HW entropy defined by Eq. (20) takes the minimum value 1 for the perturbative vacuum state as

$$S_{\text{HW}}(\{\omega\}) \geq S_{\text{HW}}(\{\omega\})\Big|_{|0\rangle,|0\rangle} = 1. \quad (\text{D7})$$

To show the above inequality, we utilize the theorem given in Refs. [68,69] stating that, in general, the HW entropy for given conjugate variables (\hat{x}, \hat{p}) and the smearing parameter σ takes the minimum value 1 for the coherent state $|\alpha; \sigma\rangle$ defined as the eigenstate of the “annihilation operator”, $\hat{a} = (\sigma\hat{x} + i\hat{p})/\sqrt{2\sigma}$:

$$S_{\text{HW}}(\sigma) \geq S_{\text{HW}}(\sigma)\Big|_{|\alpha; \sigma\rangle, |\alpha; \sigma\rangle} = 1. \quad (\text{D8})$$

Then, one sees that the HW entropy with the smearing width $\{\omega_k\}$ automatically takes the minimum value 1 for the coherent states $|\{\alpha_k\}; \{\omega_k\}\rangle$ defined by the annihilation operators $\{\hat{a}_k\}$ given by Eq. (16), as

$$S_{\text{HW}}(\{\omega\}) \geq S_{\text{HW}}(\{\omega\})\Big|_{|\{\alpha_k\}; \{\omega_k\}\rangle, |\{\alpha_k\}; \{\omega_k\}\rangle} = 1. \quad (\text{D9})$$

Such coherent states $|\{\alpha_k\}; \{\omega_k\}\rangle$ include the perturbative vacuum state $|0\rangle$ since it is an eigenstate of \hat{a}_k ($\hat{a}_k|0\rangle = 0$), and then

$$S_{\text{HW}}(\{\omega\}) \geq S_{\text{HW}}(\{\omega\})\Big|_{|0\rangle,|0\rangle} = 1 \quad (\text{D10})$$

generally holds.

References

- [1] P. F. Kolb, J. Sollfrank, and U. W. Heinz, *Phys. Rev. C* **62**, 054909 (2000).
- [2] P. Huovinen, P. F. Kolb, U. W. Heinz, P. V. Ruuskanen, and S. A. Voloshin, *Phys. Lett. B* **503**, 58 (2001).
- [3] D. Teaney, J. Lauret, and E. V. Shuryak, *Phys. Rev. Lett.* **86**, 4783 (2001).
- [4] T. Hirano and K. Tsuda, *Phys. Rev. C* **66**, 054905 (2002).
- [5] H. Song and U. W. Heinz, *Phys. Rev. C* **78**, 024902 (2008).
- [6] R. J. Fries, B. Muller, and A. Schafer, *Phys. Rev. C* **78**, 034913 (2008).
- [7] B. Muller and A. Schafer, *Int. J. Mod. Phys. E* **20**, 2235 (2011).
- [8] U. W. Heinz and P. F. Kolb, *Nucl. Phys. A* **702**, 269 (2002).
- [9] L. D. McLerran and R. Venugopalan, *Phys. Rev. D* **49**, 2233 (1994).
- [10] L. D. McLerran and R. Venugopalan, *Phys. Rev. D* **49**, 3352 (1994).
- [11] L. D. McLerran and R. Venugopalan, *Phys. Rev. D* **50**, 2225 (1994).
- [12] A. Kovner, L. D. McLerran, and H. Weigert, *Phys. Rev. D* **52**, 3809 (1995).
- [13] A. Kovner, L. D. McLerran, and H. Weigert, *Phys. Rev. D* **52**, 6231 (1995).
- [14] E. S. Weibel, *Phys. Rev. Lett.* **2**, 83 (1959).
- [15] S. Mrówczyński, *Phys. Lett. B* **214**, 587 (1988); **656**, 273 (2007) [erratum].
- [16] S. Mrowczynski, *Phys. Lett. B* **314**, 118 (1993).
- [17] J. Randrup and S. Mrówczyński, *Phys. Rev. C* **68**, 034909 (2003).
- [18] P. Romatschke and M. Strickland, *Phys. Rev. D* **68**, 036004 (2003).
- [19] P. Romatschke and M. Strickland, *Phys. Rev. D* **70**, 116006 (2004).
- [20] P. B. Arnold, J. Lenaghan, and G. D. Moore, *J. High Energy Phys.* **0308**, 002 (2003).
- [21] G. K. Savvidy, *Phys. Lett. B* **71**, 133 (1977).
- [22] S. G. Matinyan and G. K. Savvidy, *Nucl. Phys. B* **134**, 539 (1978).
- [23] A. Iwazaki, *Prog. Theor. Phys.* **121**, 809 (2009).
- [24] N. K. Nielsen and P. Olesen, *Nucl. Phys. B* **144**, 376 (1978).
- [25] H. Fujii and K. Itakura, *Nucl. Phys. A* **809**, 88 (2008).

- [26] H. Fujii, K. Itakura, and A. Iwazaki, Nucl. Phys. A **828**, 178 (2009).
- [27] P. Romatschke and R. Venugopalan, Phys. Rev. Lett. **96**, 062302 (2006).
- [28] P. Romatschke and R. Venugopalan, Eur. Phys. J. A **29**, 71 (2006).
- [29] P. Romatschke and R. Venugopalan, Phys. Rev. D **74**, 045011 (2006).
- [30] J. Berges, S. Scheffler, and D. Sexty, Phys. Rev. D **77**, 034504 (2008).
- [31] J. Berges, D. Gelfand, S. Scheffler, and D. Sexty, Phys. Lett. B **677**, 210 (2009).
- [32] K. Fukushima and F. Gelis, Nucl. Phys. A **874**, 108 (2012).
- [33] J. Berges, S. Scheffler, S. Schlichting, and D. Sexty, Phys. Rev. D **85**, 034507 (2012).
- [34] J. Berges and S. Schlichting, Phys. Rev. D **87**, 014026 (2013).
- [35] S. Tsutsui, H. Iida, T. Kunihiro, and A. Ohnishi, Phys. Rev. D **91**, 076003 (2015).
- [36] S. Tsutsui, T. Kunihiro, and A. Ohnishi, Phys. Rev. D **94**, 016001 (2016).
- [37] K. Dusling, T. Epelbaum, F. Gelis, and R. Venugopalan, Phys. Rev. D **86**, 085040 (2012).
- [38] T. Epelbaum and F. Gelis, Phys. Rev. Lett. **111**, 232301 (2013).
- [39] H. Tsukiji, H. Iida, T. Kunihiro, A. Ohnishi, and T. T. Takahashi, Phys. Rev. D **94**, 091502 (2016).
- [40] H. Tsukiji, T. Kunihiro, A. Ohnishi, and T. T. Takahashi, Prog. Theor. Exp. Phys. **2018**, 013D02 (2018).
- [41] J. Berges, K. Boguslavski, S. Schlichting, and R. Venugopalan, Phys. Rev. D **89**, 074011 (2014).
- [42] J. Berges, K. Boguslavski, S. Schlichting, and R. Venugopalan, Phys. Rev. D **89**, 114007 (2014).
- [43] J. Berges, K. Boguslavski, S. Schlichting, and R. Venugopalan, J. High Energy Phys. **1405**, 054 (2014).
- [44] J. Eisert, M. Cramer, and M. B. Plenio, Rev. Mod. Phys. **82**, 277 (2010).
- [45] S. Ryu and T. Takayanagi, Phys. Rev. Lett. **96**, 181602 (2006).
- [46] K. Husimi, Proc. Phys. Math. Soc. Jpn. **22**, 264 (1940).
- [47] A. Wehrl, Rev. Mod. Phys. **50**, 221 (1978).
- [48] A. Wehrl, Rep. Math. Phys. **16**, 353 (1979).
- [49] T. Kunihiro, B. Müller, A. Ohnishi, and A. Schafer, Prog. Theor. Phys. **121**, 555 (2009).
- [50] P. B. Arnold, G. D. Moore, and L. G. Yaffe, J. High Energy Phys. **0301**, 030 (2003).
- [51] J. Berges, AIP Conf. Proc. **739**, 3 (2004).
- [52] G. Aarts and J. Berges, Phys. Rev. Lett. **88**, 041603 (2002).
- [53] Y. Hatta and A. Nishiyama, Nucl. Phys. A **873**, 47 (2012).
- [54] G. Aarts and J. Smit, Phys. Lett. B **393**, 395 (1997).
- [55] G. Aarts and J. Smit, Nucl. Phys. B **511**, 451 (1998).
- [56] G. Aarts, G. F. Bonini, and C. Wetterich, Phys. Rev. D **63**, 025012 (2001).
- [57] D. Bodeker, L. D. McLerran, and A. V. Smilga, Phys. Rev. D **52**, 4675 (1995).
- [58] C. Greiner and B. Muller, Phys. Rev. D **55**, 1026 (1997).
- [59] A. Dumitru and Y. Nara, Phys. Lett. B **621**, 89 (2005).
- [60] A. Dumitru, Y. Nara, and M. Strickland, Phys. Rev. D **75**, 025016 (2007).
- [61] A. Ohnishi, H. Matsuda, T. Kunihiro, and T. T. Takahashi, Prog. Theor. Exp. Phys. **2021**, 023B09 (2021).
- [62] T. Epelbaum and F. Gelis, Phys. Rev. D **88**, 085015 (2013).
- [63] Y. V. Kovchegov, Nucl. Phys. A **692**, 557, (2001).
- [64] A. Kurkela and Y. Zhu, Phys. Rev. Lett. **115**, 182301 (2015).
- [65] A. H. Mueller and D. T. Son, Phys. Lett. B **582**, 279 (2004).
- [66] S. Jeon, Phys. Rev. C **72**, 014907 (2005).
- [67] K. Dusling, F. Gelis, and R. Venugopalan, Nucl. Phys. A **872**, 161, (2011).
- [68] E. H. Lieb, Commun. Math. Phys. **62**, 35 (1978).
- [69] E. A. Carlen, J. Funct. Anal. **97**, 231 (1991).